# FAST CHIRPED SIGNALS FOR A TDMA ULTRASONIC INDOOR POSITIONING SYSTEM

A Thesis

presented to

the Faculty of California Polytechnic State University,

San Luis Obispo

In Partial Fulfillment

of the Requirements for the Degree

Master of Science in Electrical Engineering

by

Lauren M. Williams

June 2020

COMMITTEE MEMBERSHIP

| | |
|---|---|
| TITLE: | Fast Chirped Signals for a TDMA Ultrasonic Indoor Positioning System |
| AUTHOR: | Lauren M. Williams |
| DATE SUBMITTED: | June 2020 |
| COMMITTEE CHAIR: | Vladimir Prodanov, Ph.D.<br>Associate Professor<br>Department of Electrical Engineering |
| COMMITTEE MEMBER: | Xiao-Hua (Helen) Yu, Ph.D.<br>Professor<br>Department of Electrical Engineering |
| COMMITTEE MEMBER: | Taufik, Ph.D.<br>Professor<br>Department of Electrical Engineering |

ABSTRACT

Fast Chirped Signals for a TDMA Ultrasonic Indoor Positioning System

Lauren M. Williams

In this paper, a new concept for ultrasonic indoor positioning based on instantaneous frequency of ultrasonic signals is presented. Nonlinear phase characteristics of ultrasonic transducers introduce a frequency deviation in ultrasonic signals. By sweeping at very fast rates, a large spike in the deviation is introduced. The artefacts observable in instantaneous frequency estimations are highly localized and present an opportunity for accurate frequency detection. In order to be useful, the artefacts need to take place within the pulse and have sufficient magnitude for accurate processing. The system consists of a transducer transmitter and receiver pair, which have a center frequency of 40kHz and a bandwidth of 460Hz. In order to incorporate more transmitters, a time-division multiple access (TDMA) scheme is applied to ensure orthogonality of signals. The concept includes four ultrasonic transmitters and a single receiver, which can uniquely identify each transmitter by a distinct signal sweep. Linear chirp signals are used to form narrow pulses and ensure no interference in the TDMA scheme. The received signal is amplified and passed through a phase-locked loop (PLL) to detect the chirp signals. Accurate instantaneous frequency detection can be done on the voltage-controlled oscillator (VCO) of the PLL, which has a narrower bandwidth than the overall signal sweep. The instantaneous frequency estimation methods are largely explored in this work and consider two methods: the Hilbert transform and a zero-crossings method. This work highlights some of the advantages and disadvantages of both methods. Time of flight (ToF) in this system can ultimately be obtained by considering the instantaneous frequency estimations and the time for one particular frequency to be transmitted and received.

Keywords: Ultrasonic Signals, ToF, TDMA, Instantaneous Frequency, Hilbert Transform, Nonlinear Phase

# ACKNOWLEDGMENTS

I would like to sincerely thank my advisor Dr. Vladimir Prodanov for all of your guidance, patience, and effort. I appreciate all the time you took to explain concepts to me throughout the year. Whether it was in your office or over Zoom, you always helped me learn and be excited about my work.

I would like to thank Dr. Xiao-Hua (Helen) Yu and Dr. Taufik. Thank you both for being on my committee. I have truly enjoyed being in your classes throughout the years.

I would also like to give thanks to Kyman Huang. Thank you for being one of my best friends in and out of school. You have been my study buddy throughout school and someone I could always turn to for technical advice. Thank you for laughing with me and calming me down when simulations wouldn't run, chips broke, and measured data made no sense.

I would like to thank my family, Xiaoying Yu, David Williams, and Janelle Williams, for their support and encouragement throughout my time at Cal Poly. It would not have been possible for me to pursue my master's degree in electrical engineering without them. A special thanks to my mom, Xiaoying Yu, for inspiring me to follow her footsteps in becoming an electrical engineer.

TABLE OF CONTENTS

Page

LIST OF TABLES

Table Page

LIST OF FIGURES

Figure Page

# Chapter 1

# INTRODUCTION

Indoor ultrasonic positioning systems have become relevant and popular because they outperform traditional RF location finding systems in terms of accuracy and cost. A significant advantage of ultrasound is the slower propagation speed of sound waves compared to electromagnetic waves in RF systems. This allows for the hardware implementation to be simpler and cheaper. Additionally, the use of ultrasound in location finding is not new. The echolocation system used by bats and other animals is highly accurate. Echolocation systems are a template for modern indoor positioning systems due to its precision and ability to overcome complex navigation issues. Ultrasound is also an appealing method for location finding for technology developers since ultrasonic systems do not require any specific network setup. The technology and diversity of ultrasonic systems are continuing to grow as companies increasingly find more and more applications for it.

This thesis presents a new concept that incorporates the use of unique, frequency modulated signals for distance measurements. The following sections will describe relevant features and technical specifications.

## 1.1 Ultrasound and Ultrasound Positioning Systems

Ultrasound refers to sound generated above the human hearing range [1]. Ultrasonic signals typically range from 20kHz to 50MHz. Devices that transmit and receive electrical energy in the form of sound are called ultrasonic transducers. Since ultrasonic waves have higher frequencies than audible sound, it also has a shorter wavelength. This makes ultrasound useful for measuring distances with higher precision. The new technology employing ultrasonic transducers now demand millimeter range of operation [2]. There are two primary ways to measure distance using ultrasonic transducers; they are time of flight (ToF) and the amplitude of the received signal [3][4]. Time of flight also known as time of arrival (ToA) can be defined as the time it takes for a signal to leave the transmitter and arrive at the receiver. Given that the speed of sound in air is $343\frac{m}{s}$ at room temperature and atmospheric pressure, the distance can be calculated by $d = vt$, where $d$ is distance and $t$ is time of flight. This assumes ideal conditions and

no changes of sound velocity due to temperature, pressure, or humidity. In nonideal conditions, the speed of sound in a gas can be calculated from [5]:

$$v_o^2 = \gamma \frac{RT}{M}\left(1 + \frac{2pB}{RT}\right) \tag{1.1}$$

In this equation, $v_o$ is the speed of sound, $\gamma$ is the specific heat ratio ($\frac{c_p}{c_v}$), $R$ is the universal gas constant, $T$ is temperature in K, $M$ is Molar mass, $p$ is pressure, and $B$ is the second virial coefficient (given). In addition, given that the speed of sound is $343\,\frac{m}{s}$, wavelength $\lambda$ of a signal can be found by:

$$\lambda = \frac{v}{f} \tag{1.2}$$

This equation implies that at higher frequencies, wavelength is shorter and distance resolution improves.

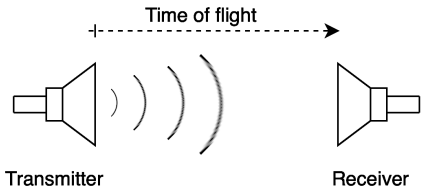


Figure 1: Time of flight between ultrasonic transmitter and receiver is proportional to distance

There are three primary time of flight systems that exist using ultrasonic transducers. They are shown in figure 2. The first has a co-located transmitter and receiver to locate objects or obstacles. This is the method used in echolocation. The second time of flight system uses separated transmitters and receivers. Ultrasonic flow meters are one example of this type of system. The last time of flight system uses multiple transmitters and a single receiver. This method is used in most ultrasonic positioning systems including the one discussed in this thesis.

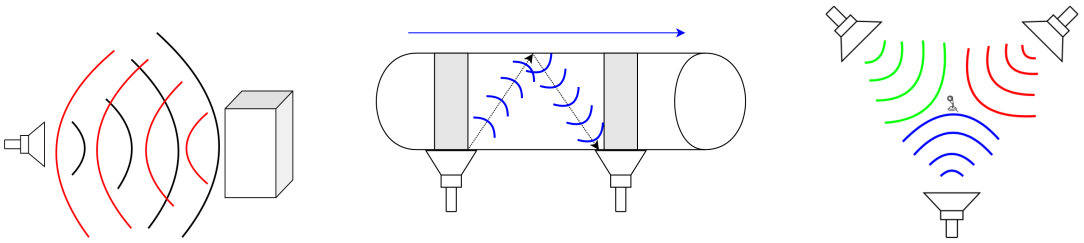

(a) (b) (c)

Figure 2: Time of flight systems showing co-locating Tx and Rx with an object (a) separated Tx and Rx (b) and multiple Tx and single Rx (c)

As already stated, the idea of using sound waves for location information is not new to nature. Bats, dolphins, and several other animals use echolocation for navigation. Bat echolocation is most interesting and well-studied because bats use a varying frequency range, both constant and modulating frequencies, different bandwidths, varying pulse durations, fluctuating call intensity, and more [6]. Bat echolocation call frequencies vary species to species but are approximately between 11kHz and 212kHz. Insect eating bats transmit calls between 20kHz and 60kHz because lower frequencies do not have short enough wavelengths to detect accurate locations for small bugs.

In figure 3, $P_{out}$ represents the acoustic pressure disturbance of the emitted signal, $P_{echo}$ is the pressure disturbance of the backscattered signal, and $P_{ear}$ is the pressure signal reaching the bat's ear. $P_{ear}$ as well as the time of flight of the reflected signal to both ears, contribute to knowing $\theta$, the angle indicating where the object of interest is. The echolocation system used by bats is remarkable since bats place their calls at one location and hear the echo at a different place in their flight trajectory. In addition, the Doppler effect will alter the perceived frequencies when the bats are moving. Despite these challenges, by being able to interpret transmission, reflection, and reception variables, bats can effectively determine size, distance, and location of objects around them.

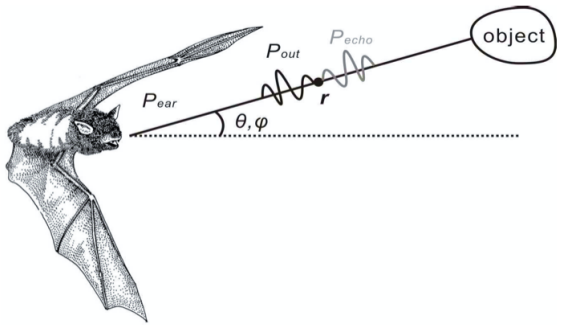

Figure 3: Diagram of a bat's echolocation system [7]

Another well-known system that utilizes the concept of co-locating a transmitter and a receiver is ultrasound imaging. Ultrasonic imaging is a powerful tool for modern medicine as it reveals images and information about internal organs, blood flow, and other aspects of the human body. Compared to other forms of radiation in medical imaging, ultrasonic signals are nonionizing, which makes it much safer for patients as well as for doctors [8]. In ultrasonic imaging, piezoelectric transducers are used. These transducers work by exposing piezoelectric crystals to small currents to transmit ultrasonic pulse signals.

The crystals also produce a small current when they are affected by reflected ultrasonic waves [9]. Therefore, the image produced is a display of reflecting surfaces within the body.

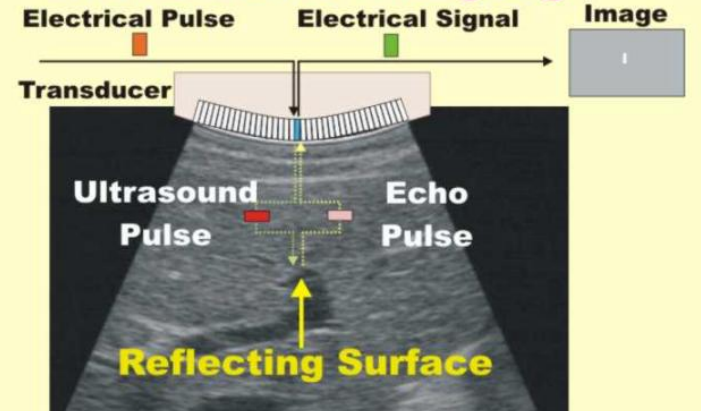

Figure 4: Ultrasound Imaging Process [10]

Mobile robots are used in an array of applications such as floor cleaners and domestic service robots [11], navigation tools in buildings, service guides for the elderly [12], and more. In each of these systems, some means of obstacle avoidance is essential. Co-located transmitters and receivers are used on many robots for estimating the distance to objects and collision avoidance.

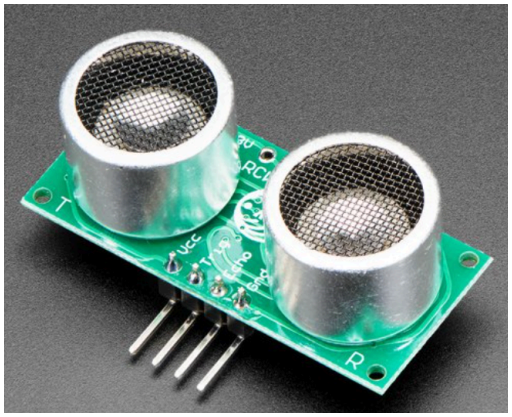
Figure 5: Ultrasonic distance sensors with co-located transmitter and receiver used in robotics applications [13]

A different ToF method that can be used as a medical tool includes separate transmitters and receivers. This method is most commonly used in ultrasonic flow meters. Ultrasonic flow meters use ultrasound signals to determine the velocity of a fluid flowing in a pipe [14]. In medical applications, the

"pipe" of interest is usually blood vessels, and flow meters can determine the velocity of blood flow. The system works by propagating ultrasonic signals upstream and downstream through the pipe. By measuring the difference in travel time of the signal from the transmitter to the receiver and knowing the size of the pipe, the ultrasonic flow meter can determine the velocity of the liquid and the flow rate [15]. Flow meters have also been used for gas flow rate measurement.

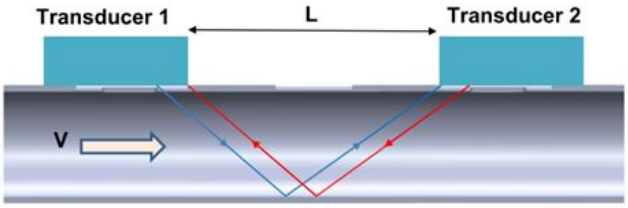


Figure 6: Ultrasonic flow meter with separate transducer and receiver [16]

The last ToF method uses multiple transmitters and a single receiver. This method is used in ultrasonic indoor positioning systems. In an indoor, localized environment, an object of interest that is to be located would contain the receiver. Multiple transmitters are used to improve accuracy and the transmitted signals must be orthogonal, meaning they do not interfere. Orthogonality differs depending on the communication scheme. In a system where ultrasonic signals are pulses, systems allocate time slots for each active ultrasonic transducer [17]. This communication scheme is known as time-division multiple access (TDMA). Scheduling the transmitted pulses in a collision free manner eliminates configuration issues.

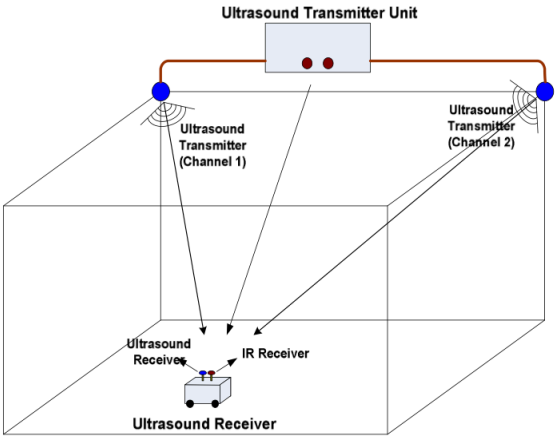


Figure 7: Ultrasonic positioning system with multiple transmitters and a single receiver [18]

1.2 Ultrasonic Transducers and Band-pass Signals

Ultrasonic transducers are band-limited devices with a central frequency and bandwidth associated with its input impedance, which can be modeled as an RLC circuit [19]. The RLC circuit model can be used to describe a transducer's behavior when it is operating at its resonant frequency. In figure 8, $V_2$ represents the acoustic signal transmitted by the piezoelectric crystal as well as other losses by the crystal. $L_1$ and $C_1$ represent the resonant components. The parallel capacitor $C_o$ represents the dielectric in the transducer, which is the piezoelectric material.

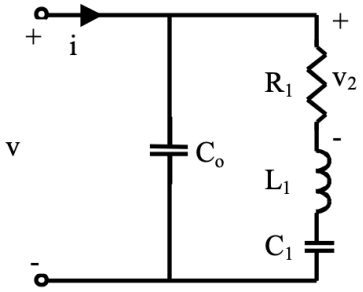


Figure 8: Equivalent RLC circuit model for a piezoelectric transducer [19]

The total impedance of the circuit can be computed [20]:

$$Z_{tot}(s) = \frac{s^2 L_1 C_1 + sC_1 R_1 + 1}{s^3 L_1 C_1 C_2 + s^2 C_1 C_2 R_1 + sC_2 + sC_1} \tag{1.3}$$

The magnitude of the impedance can be solved as:

$$|Z_{tot}|(\omega) = \frac{\sqrt{(1-\omega^2 L_1 C_1)^2 + \omega^2 C_1^2 R_1^2}}{\sqrt{\omega^4 C_1^2 C_2^2 R_1^2 + \omega^2 (C_1 + C_2 - \omega^2 L_1 C_1 C_2)^2}} \tag{1.4}$$

Using 'solve' in Microsoft Excel, the model parameters $R_1$, $L_1$, $C_1$, and $C_2$ can be obtained from the measured $Z(s)$ of a particular transducer. For example, the values in table 1 correspond to the transducer MSO-P1040H07T. Although these transducers are not exactly the same as the ones used in this work (40TR-12B), these values result in nearly the same $Q$ and $\omega$ values. Therefore, the numbers used in the impedance model are representative of what would be seen for the transducers used in this work.

Table 1: Transducer Equivalent Impedance Values Modeling the Operation of the MSO-P1040H07T

| $R_1$ | $L_1$ | $C_1$ | $C_2$ |
|---|---|---|---|
| 370Ω | 74.5mH | 213pF | 2.2nF |

The transfer function of the circuit can be solved by solving for the voltage across resistor $R_1$. The voltage across this model component is relevant because the electrical energy lost to this component accounts for the loss in the electric-to-acoustic conversion. The capacitor $C_2$ can be disregarded for this calculation since it is in parallel, and we assume the circuit is voltage driven. The transfer function can be written as:

$$V_{R_1}(s) = \frac{R_1}{R_1 + sL_1 + \frac{1}{sC_1}} V_{in} \tag{1.5}$$

By converting this transfer function to the frequency domain, the frequency and magnitude response can be obtained.

$$H(\omega) = \frac{j\omega C_1 R_1}{-\omega^2 L_1 C_1 + j\omega C_1 R_1 + 1} \tag{1.6}$$

$$|H(\omega)| = \frac{\omega C_1 R_1}{\sqrt{(1-\omega^2 L_1 C_1)^2 + (\omega C_1 R_1)^2}} \tag{1.7}$$

The frequency response equation shows that the electric-to-acoustic transduction is a bandpass process. It can be rewritten to acquire the center frequency $\omega_o$ and the quality factor $Q$.

$$|H_{BP}(\omega)| = \frac{1}{\sqrt{1 + Q^2(\frac{\omega_o}{\omega} - \frac{\omega}{\omega_o})^2}} \tag{1.8}$$

Using the equations: $Q = \frac{\sqrt{L/C}}{R}$ and $\omega_o = \frac{1}{\sqrt{LC}}$, $Q$ can be computed as 50 and $\omega_o$ can be computed as $2.5 \times 10^5 \ \frac{rad}{sec}$ or $f_0 = 39.95kHz$. With a Q of 50, the transduction process is relatively narrow band with a bandwidth of around 800Hz.

Band-pass signals are waveforms that are frequency limited to a particular range. As previously discussed, ultrasonic transducers act as a form of bandpass filter due to their limited bandwidth capabilities. In the system described in this thesis, the transmitted signal is greatly impacted by the acoustic channel and the high order filtering that results as it passes through the transducers. The frequency dependence introduced by the transducers can be described as a fourth order filter and this will be discussed in more detail in chapter 4.

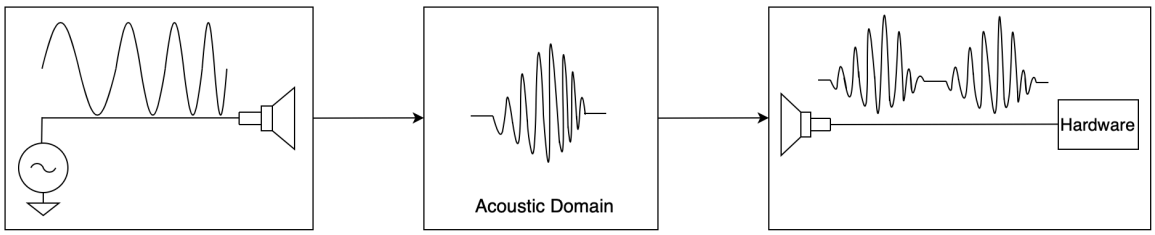


Figure 9: Block diagram illustrating signal going from electrical to acoustic, through the acoustic channel, and acoustic back to electric

A fourth order bandpass filter is used to model the 40TR-12B [21] transducer transmitter and receiver with a second order response associated with each device. There are two quality factor values for the model of this system since the transmitter and receiver are both treated as second order filters. These quality factors are: $Q_1 = 55.94,\ Q_2 = 57.95$, and will be discussed more in chapter 4. The magnitude and phase responses of the fourth order response created by the 40TR-12B pair are plotted in figure 10. From the magnitude response, the 3dB bandwidth of the Tx-Rx pair is from 40.06kHz to 40.52kHz, which is 460Hz.

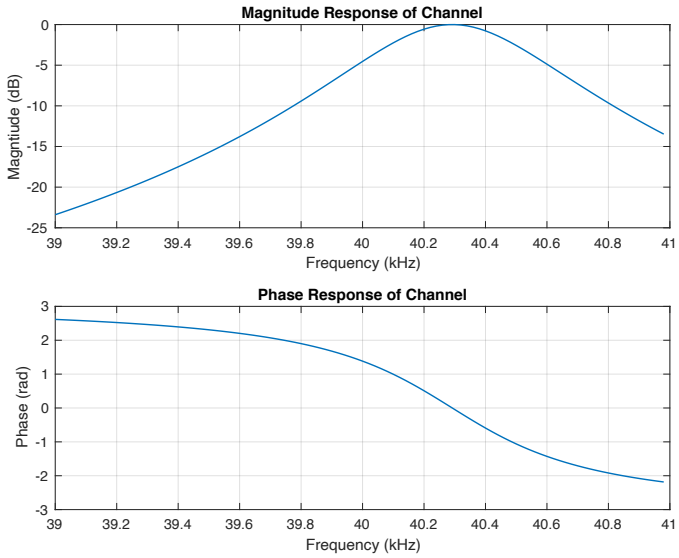


Figure 10: Magnitude and phase response of fourth order bandpass model of 40TR-12B Tx-Rx

The impulse response of the fourth order filter representation of the ultrasonic transducers is shown in figure 11 and the step response is shown in figure 12. The duration of both responses are approximately

3ms. The impulse response shows that the filter takes around 3ms to reach steady state. This would suggest that signals that could be used with such a system would have a duration of at least 3ms, which is the duration of the impulse response.

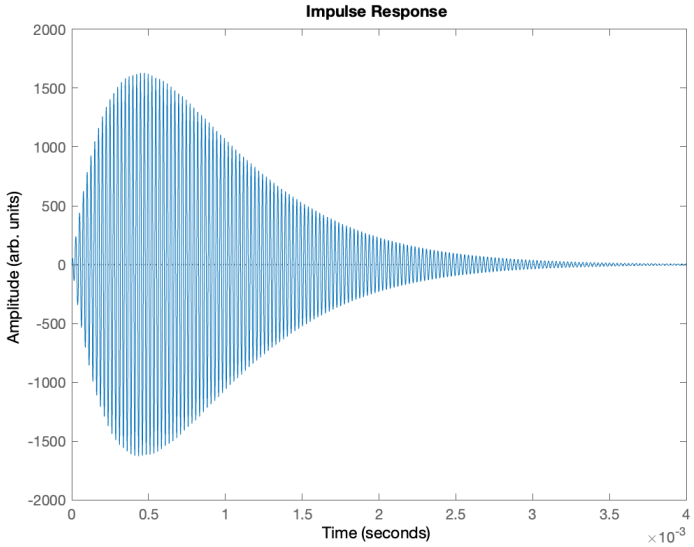


Figure 11: Fourth order bandpass model of 40TR-12B Tx-Rx impulse response

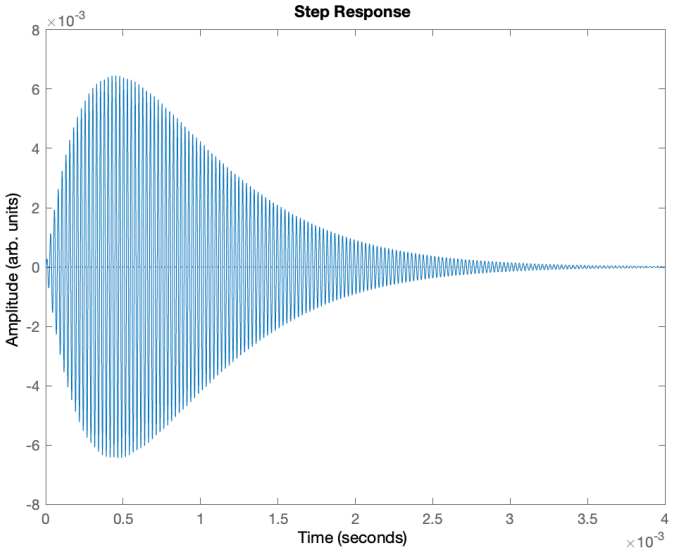


Figure 12: Fourth order bandpass model of 40TR-12B Tx-Rx step response

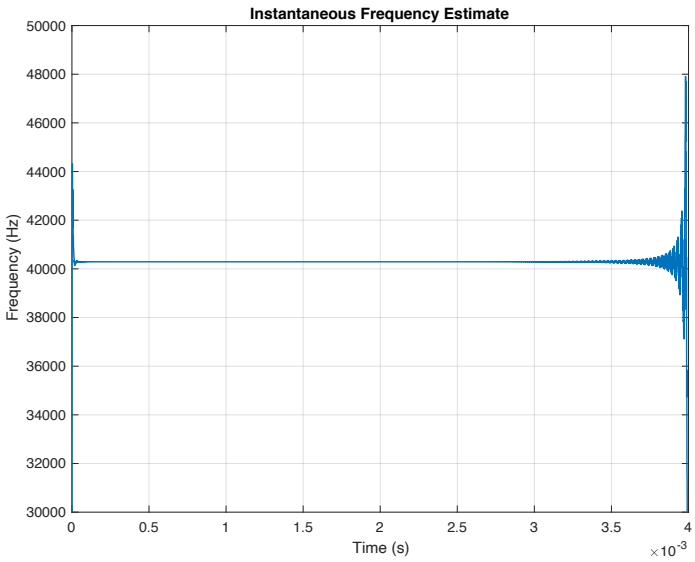

Figure 13: Instantaneous frequency plot of the step response

With a given system $H(s)$ taking the inverse Laplace transform of the transfer function will result in the unit impulse response of the system [22]. The impulse response $h(t)$ can be found:

$$h(t) = \mathcal{L}^{-1}\{H(s)\} \tag{1.9}$$

The impulse response can also be found by taking the derivative of the step response $y_\gamma$. Since the impulse response is the output of an impulse $\delta(t)$ being passed through a system, the impulse response can be denoted as $y_\delta(t)$.

$$y_\delta(t) = h(t) = \frac{d}{dt} y_\gamma(t) \tag{1.10}$$

The instantaneous frequency of the step response shows a near constant frequency around 40kHz. This implies that the filter's natural frequency rings around 40kHz and does not appear to change during the pulse.

This filter can also be analyzed in the frequency domain. The magnitude and phase response are illustrated in figure 10. The center frequency shown in the frequency response is $2.53 \times 10^5 \frac{rad}{s}$, or $40.266kHz$.

In addition, the impulse response plot is non-symmetric. This suggests that the filter does not have linear phase. The phase response shown in figure 10 confirms this.

## 1.3 Thesis Statements

This thesis explores a new system that incorporates the use of unique, linearly sweeping (chirp) [23] signals for a TDMA configured ToF localization system. Each linear sweep generates a frequency modulated (FM) pulse by sweeping through the operating frequency range of the transducers. This sweep is such that the duration of the produced FM pulse approaches the duration of the system's impulse response. Two sweep patterns are examined- an up-sweep and a down-sweep. Instantaneous frequency measurements determine which pattern was transmitted and therefore which transmitter it was coming from. These measurements also indicate ToF and therefore distance. This system attempts to address various issues that arise including artefacts in the instantaneous frequency, as well as non-linear phase distortion. The artefacts that occur in fast sweeping signals can potentially be used for accurate frequency detection.

## 1.4 Thesis Organization

In this thesis, a new approach to ultrasonic positioning will be discussed as well as some previous approaches to indoor positioning. This paper is organized as follows. Chapter 2 discusses indoor positioning systems and chirp signals. Previous works that have inspired this research will be discussed in chapter 3. With this background on indoor positioning systems and previous implementations, the proposed system design and signaling for a new ultrasonic chirping system will be introduced in chapter 4. MATLAB simulations will also be examined in this chapter and linked to various sweeping rates, instantaneous frequency expectations, and envelope shapes. Hardware implementations and system architecture will be shown in chapter 5. These results will illuminate shortcomings in this system, which will be discussed in chapter 6. Lastly chapter 7 concludes findings and discusses challenges faced in this research.

# Chapter 2

# BACKGROUND

## 2.1 Indoor Positioning

Advancements in new technologies have increased demands for accurate indoor positioning systems. GPS is a widely used satellite-based navigation tracker, however it becomes unreliable indoors when satellite signals are unavailable. This is because RF signals cannot penetrate through roofs or walls [24]. Indoor positioning aims to allow users to have accurate navigation in a localized indoor space. There are a wide variety of applications for indoor positioning systems including: accessibility aids for the visually impaired, inventory management, location finding in hospitals of medical personnel or equipment, and more [25] [26]. The ability to locate objects or individuals has become increasingly significant in the age of automation and with the rising number of "intelligent" applications.

There are many different technologies that explore the idea of indoor positioning including: RF, Wi-Fi, RFID, mobile networks and more. A detailed survey of wireless indoor positioning systems was carried out in 2007 that details the use of GPS, RFID, cellular-based, UWB, WLAN, Bluetooth, and other location finding technologies [27]. Many of these existing solutions tend to be costly in terms of money, time for installation and maintenance, space in terms of hardware size, and energy usage. Additionally, most of these systems are best used in specific applications or environments since they are limited in either scalability or accuracy. Despite differences in these varying technologies, the fundamental components of location finding systems are the same: a distance/location measuring method, and a physical location sensor infrastructure.

The wireless technologies discussed previously including Wi-Fi, RFID, and Bluetooth, use electromagnetic waves. A significant flaw of using electromagnetic waves in location finding systems is the effect of field distortion due to eddy currents [28]. Eddy currents are induced by nearby metals when the electromagnetic field changes. The distortion can cause errors as large as several feet, which is substantial for systems requiring accuracy. The sensitivity to the ambient electromagnetic environment makes electromagnetic waves an unreliable position tracking technology for systems requiring high accuracy.

Additionally, systems that use electromagnetic signals can have large position errors as a result of small timing errors. This is because the velocity of an electromagnetic wave in free space can be defined as

the speed of light, $3 \times 10^8 \frac{m}{s}$ [29]. To illustrate this, the distance error is calculated if there is a timing error of $1\mu s$:

$$d = vt = \left(3 \times 10^8 \frac{m}{s}\right)(1\mu s) = 3m$$

This indicates that there could be an error in distance estimation of $3m$ if there is a mere $1\mu s$ timing error. Since ultrasonic transducers transmit acoustic signals, the velocity is the speed of sound, which is $343 \frac{m}{s}$. Given the same timing error of $1\mu s$, the ultrasonic system would result in a distance error of $0.34mm$, nearly 10,000 times smaller.

A positioning system uses multiple distances to determine location. Triangulation is a well-known positioning system that uses a known distance between two points as well as the measured angles from those two points to an object [30]. Trilateration is another common positioning system and it is the method used in GPS systems. The positioning methods that will be discussed in this thesis are trilateration and multilateration. In an N dimensional space, N+1 transmitters are required to locate a target based on distance measurements. Figure 14 shows an example of a position calculation in a 2D environment. The three transmitters propagate signals within their respective radii that can be received by the target. Given that the receiver is on the circle, the radius of the circle is the distance between the transmitter and receiver [31]. Two transmitter circles will intercross to produce two possible location estimations of the receiver. The third transmitter is needed to identify an exact location.

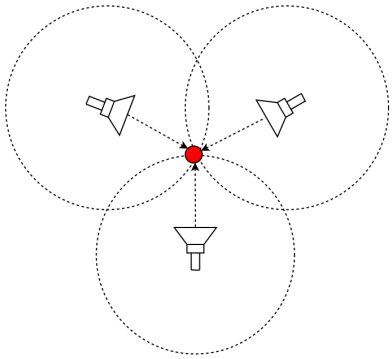

Figure 14: Trilateration position calculation in a 2-dimensional space

## 2.2 Multiple Access Techniques

A channel in a communication system refers to a system that allocates frequency channels, time slots within frequency bands, and distinct codes [32]. In the channel, users can communicate and transmit signals within a given network with minimal interference. When signals within the same channel do not interfere, they are known as orthogonal. Orthogonality can be achieved when the cross-correlation between any two sequences remain low throughout [33]. The cross-correlation vector can be written as [34]:

$$c(\tau) = \int_{-\infty}^{\infty} x(t)\, y(t+\tau) dt \tag{2.1}$$

If either signal $x(t)$ or $y(t+\tau)$ is finite while the other is zero, and the cross correlation will be zero. This scenario describes orthogonal signaling known as time division multiple access (TDMA).

Multiple access channels are communication channels that are optimized by an access method. The most common channel access schemes are frequency division multiple access (FDMA), code division multiple access (CDMA), and the previously mentioned time division multiple access (TDMA).

The FDMA scheme divides a bandwidth into multiple frequency channels. This implies that the transmitted signals need to fall within the bandwidth allocated to them. The transmitted signals are modulated by subcarriers and then demodulated at the receiving end. The primary benefit to using an FDMA scheme is that signals can be transmitted at the same time, since they operate at different frequencies.

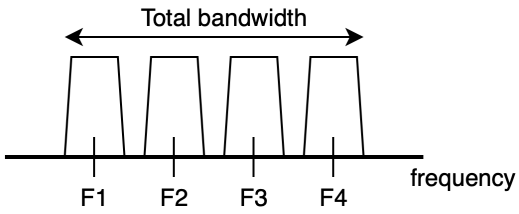


Figure 15: FDMA scheme divides bandwidth into frequency channels

The TDMA scheme divides a channel into time slots as opposed to frequency slots in the FDMA scheme. Although transmitting can only be done by one transmitter at a time, these signals can occupy the same frequency ranges. Each transmission is allocated a short period of time, and since the process of switching between different transmitters is so fast, it does not necessarily become a limitation.

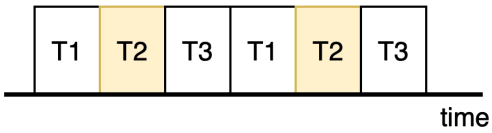

Figure 16: TDMA scheme allocates a time slot for each signal

The CDMA scheme is based on spread spectrum technology. Spread spectrum is a communication system in which the signal bandwidth is intentionally spread over a larger bandwidth [35]. As a result, the energy of the signal is spread over a larger bandwidth and appears as noise. While this technique makes the signal more difficult to distinguish, it also makes it more difficult to intercept. Only the demodulator knows the "key" or the code, and since the signal is indistinguishable from noise, the code is referred to as pseudo noise [36]. By assigning each transmitter to a distinct code, signals can overlap in time and frequency, but the CDMA scheme accomplishes orthogonality by having low cross correlation. GPS systems use the CDMA scheme and in particular they use Gold codes [37]. Orthogonality means that the dot product of the codes equals zero, but in this case the dot product must remain low for all possible time shifts to result in a low cross correlation. This method allows signals with orthogonal codes to be transmitted simultaneously.

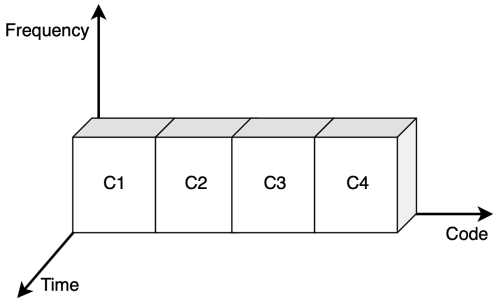

Figure 17: CDMA scheme

## 2.3 Chirp Signals and Instantaneous Frequency

In bat echolocation systems, bats can emit calls with a constant frequency or with frequency modulation. They use constant frequencies for detection and classification of object, while they use modulating frequencies for accurate localization of targets [38]. In this work, frequency modulated signals will be implemented for accurate positioning.

A chirp signal is a sinusoid whose frequency changes with time. Figure 18a illustrates a linear up-chirp signal, meaning the frequency increases linearly with time. Down-chirp sweeps are also common and as the name suggests, the frequency decreases with time. A sinusoid with constant magnitude and constant (instantaneous) frequency can be seen in figure 18c for comparison. Chirp signals are used in existing location finding systems including radar and sonar, for Pulse Compression. Pulse Compression is used to increase range resolution and receiver sensitivity [39]. The name Pulse Compression comes from the correlation of the received signal to their original chirps. When linear chirps are filtered, the signal magnitude does not decrease, but the chirp is highly compressed. This method makes the signal easier to detect and significantly improves range resolution as SNR is increased.

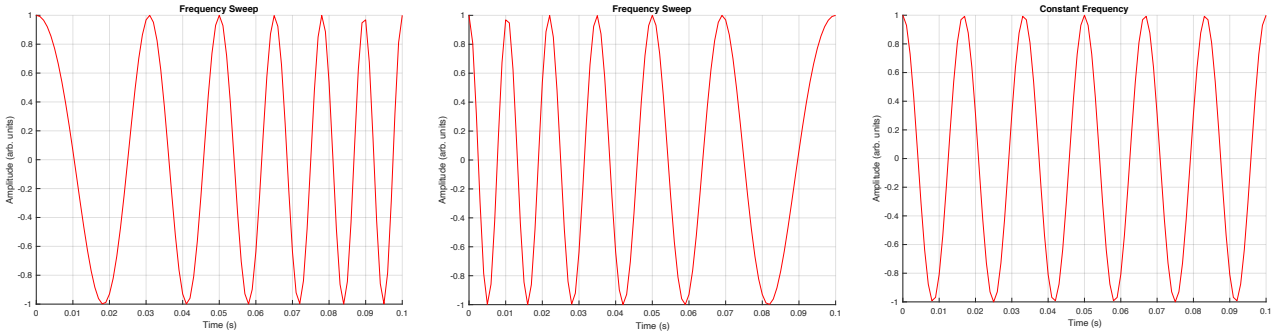


(a) (b) (c)

Figure 18: Linear up-chirp signal (a) linear down-chirp (b) and a constant frequency sinusoid (c)

The frequency of a chirp signal at a point in time can be described by its instantaneous frequency. The concept of instantaneous frequency is significant for describing nonstationary signals, whose frequencies vary with time. Linear chirp signals, which are used in this work, are one example of nonstationary signals.

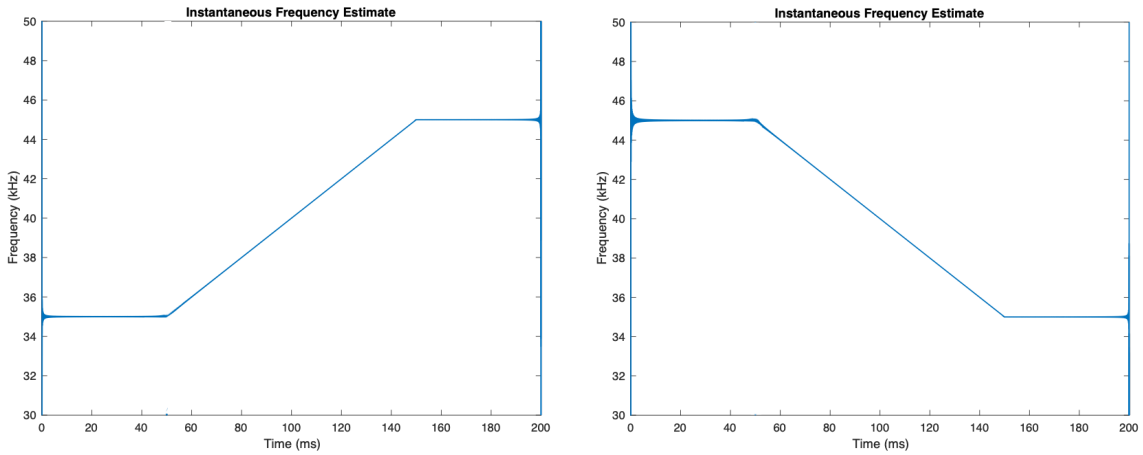


(a) (b)

Figure 19: Instantaneous frequency plot of a 10kHz, 100ms linear up chirp sweeping from 35kHz-45kHz (a) and a 100ms linear down chirp sweeping from 45kHz to 35kHz (b)

In the analysis of instantaneous frequency, it is significant to mathematically define it, as there are many interpretations. Van Der Pol started by analyzing the equation for simple harmonic motion [40]:

$$s(t) = a\cos(2\pi ft + \theta) \tag{2.2}$$

In this equation, the phase component can be understood as:

$$\phi(t) = (2\pi ft + \theta) \tag{2.3}$$

Van Der Pol created an expression for frequency modulation by reasoning a new expression for harmonic oscillations. The expression for harmonic oscillations emphasizes the phase in the cosine function and is written as:

$$s(t) = a\cos\int_0^t 2\pi f_i(t)dt + \theta \tag{2.4}$$

This led to the definition of instantaneous frequency:

$$f_i(t) = \frac{1}{2\pi}\frac{d\phi(t)}{dt} \tag{2.5}$$

Gabor developed a complex representation of a real signal by focusing on amplitudes belonging to real frequencies and suppressing those of negative frequencies. The complex signal was written as:

$$z(t) = s(t) + jH[s(t)] = a(t)e^{j\phi(t)} \tag{2.6}$$

Here, $s(t)$ is the real signal and $H$ is the Hilbert transform. The Hilbert transform is defined as:

$$H[s(t)] = p.v.\int_{-\infty}^{+\infty} \frac{s(t-\tau)}{\pi\tau} d\tau \tag{2.7}$$

In this equation p.v. describes the Cauchy principle value of the integral. Because the Hilbert transform is defined over all time, the instantaneous frequency is not a localized quantity.

As an example, the step response of the system is a sinusoid with slowly varying amplitude. The plot in figure 20b shows the instantaneous frequency of the step response of the filter.

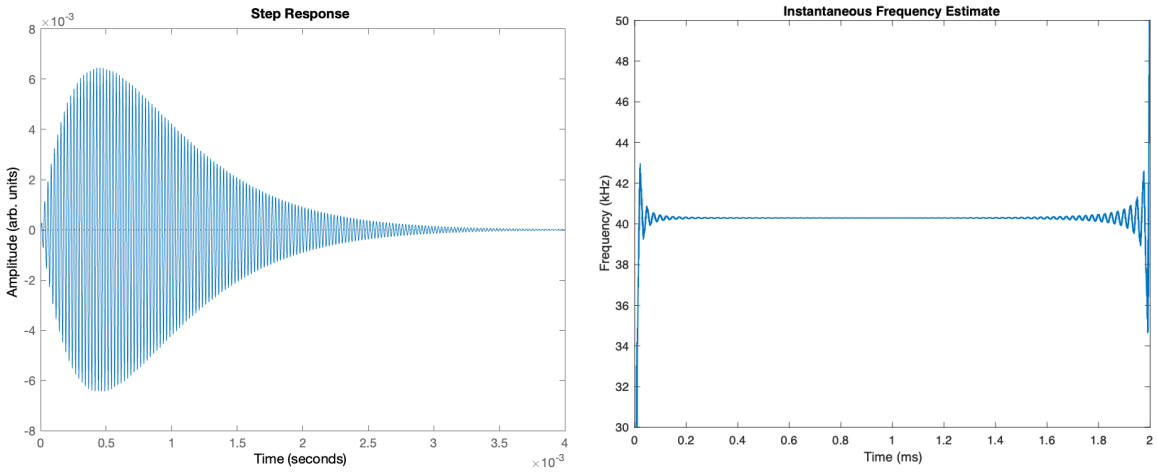


(a) (b)

Figure 20: The step response (a) and instantaneous frequency plot of step response (b) for a fourth order bandpass filter representing band limiting characteristics of ultrasonic transducers Tx and Rx

In a pulse that is generated from an up sweep from 35kHz to 45kHz, most of the energy occurs in the vicinity of 40kHz. It is possible for the pulse to be clipped, preventing the calculation of instantaneous frequency by using the Hilbert method.

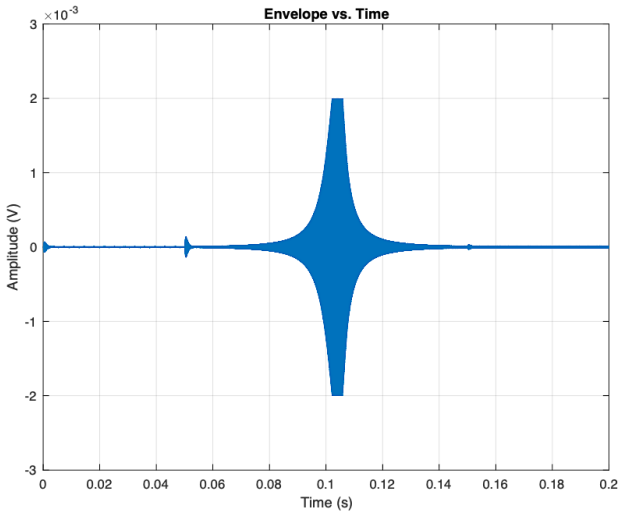


Figure 21: Clipped pulses can occur when the transmitter and receiver are too close, and the signal amplitude is large

The clipped signal within the envelope is no longer perfectly sinusoidal and is now flat on the top and bottom of each period that is clipped. Using the Hilbert transform will no longer work here, as the Hilbert transform is based on sinusoidal oscillations. Figure 22 shows the attempt of using the Hilbert transform on the clipped signal. The instantaneous frequency estimate is accurate until the clipped portion of the envelope. The clipped duration shows a large spike in the instantaneous frequency plot. Should the instantaneous frequency of the waveform be necessary for a system, alternative methods for calculating that frequency might be needed.

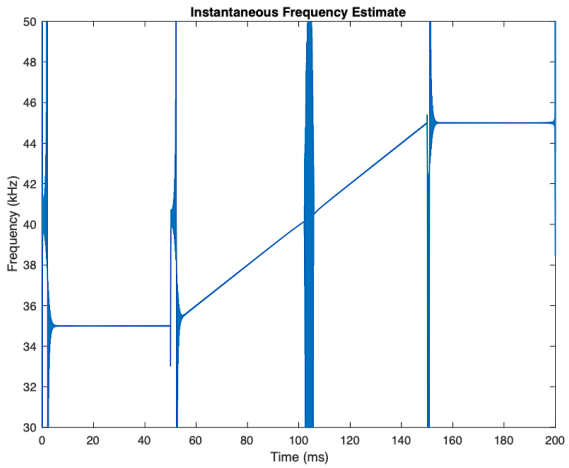


Figure 22: Using the Hilbert transform on a clipped signal reveals a large spike where the signal is clipped as the pulse signal is no longer a perfect sinusoid

Another method for measuring instantaneous frequency can be employed here where the Hilbert transform is not an option. This technique simply measures the duration between two consecutive zero crossings of a periodic signal and inverts it. It works with sinusoids and square waves alike, which is useful in cases where a signal could be clipped. This method will be described more in chapter 4.

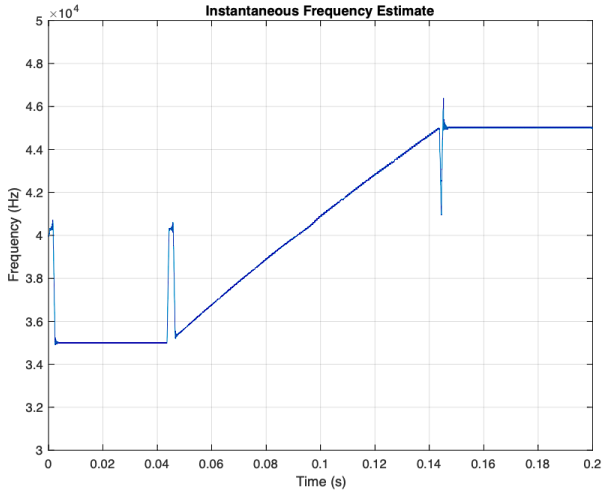


Figure 23: Instantaneous frequency estimate of a clipped pulse using the zero crossings method

Figure 24 shows the instantaneous frequency plots using both methods. The Hilbert transform method is shown in blue and the zero-crossings method is shown in red.

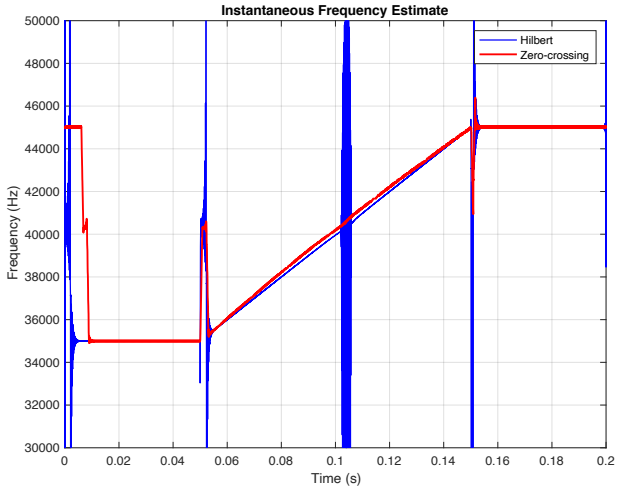


Figure 24: Comparing instantaneous frequency plots using the Hilbert transform (blue) and the zero-crossing method (red)

# Chapter 3

# LITERATURE REVIEW

Within the field of indoor positioning systems (IPS), there are many different approaches to ToF measurements, distance estimations, transmitter synchronization, correlation, communication schemes and more. This chapter discusses a few significant works that have inspired the research done in this thesis.

## 3.1 TELIAMADE

An example of a system that uses ultrasonic signals to estimate time of flight is the TELIMADE system [41]. In this system, the time of flight measurement is obtained by estimating using a quadrature detector as well as the time instant at which the envelope reaches its maximum value. A quadrature detector is used to optimize memory requirements and reduce computational costs. The quadrature detector is a popular frequency modulation detector that mixes the original signal with a 90-degree phase shifted version of the signal [42]. The output of the mixer acts as a phase detector and produces a voltage output proportional to the phase difference. Parabolic interpolation and phase correction are used to further increase accuracy in ToF estimation. From the in-phase and quadrature components of the quadrature detector, the phase can be calculated with the assumption that signal delay can be estimated as in integer number of wavelengths. This phase information provides a correction to the ToF estimation to make it more accurate.

However, a problem may occur if the transmitter and receiver are too close, and the receiver detects a signal with a large amplitude that could potentially be clipped. If this is the case, the TELIMADE system would not be able to detect a maximum value of the envelope and would no longer be able to estimate time of flight.

The transducers used in the TELIAMADE system are 400ST/R120 with a 40kHz center frequency and a 6dB bandwidth of 2kHz.

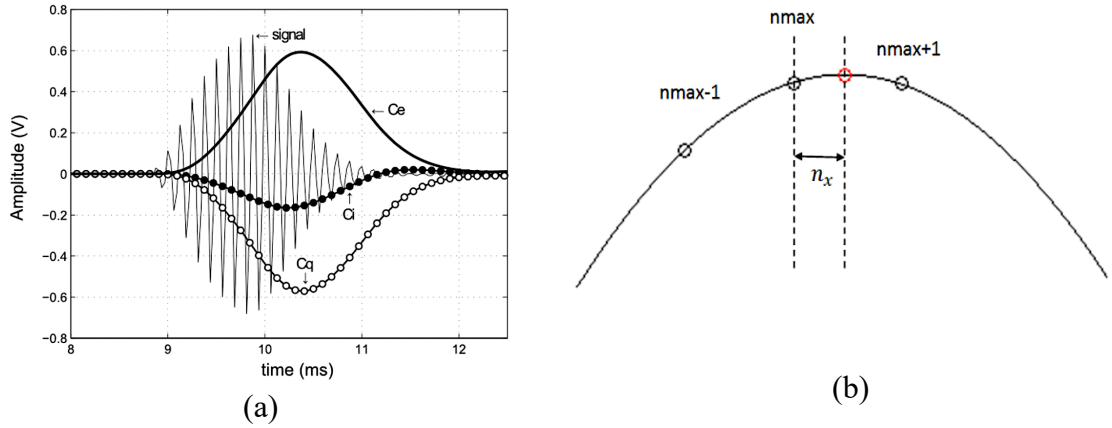


(a) (b)

Figure 25: Reception of an ultrasonic pulse (a) and parabolic interpolation to obtain the maximum value of the signal envelope (b)

3.2 Indoor Pseudo-ranging of Mobile Devices using Ultrasonic Chirps

Another system uses a time difference of arrival (TDOA) pseudo-ranging technique in which each transmitter simultaneously sends a unique encoded message, which arrive at different times [43]. The time difference information can remove the requirement of knowing exactly when a signal was transmitted.

This method utilizes the same approach as radar, using Pulse Compression on linear chirp signals. Transmitters are uniquely identified by having specific chirping rates and maintain orthogonality using CDMA also known as Chirp Spread Spectrum (CSS). An example of the chirping rates can be seen in figure 26a. This system is at the edge of the audible range, so in order to eliminate any noises that could be perceived, each chirp is slowly faded in and faded out. This results in long chirp signals with long settling times. The sweep range for all of the chirps was from 19kHz to 23kHz. The transmitters used in this system were the Goldwood GT-1016 Dispersion Piezo Horn Tweeters. These transmitters have a frequency range from 3.5kHz to 27kHz. This range is between sonic and ultrasonic.

In addition, this system requires receivers and transmitters (speakers and potentially phones) to support frequencies up to 24kHz, and this is a significant limitation for some smart phones and some modern sound systems.

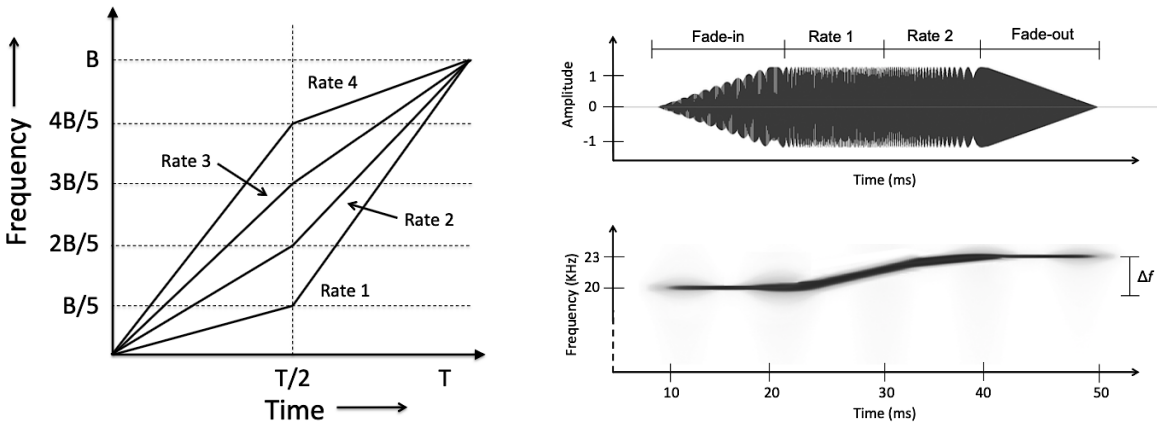


Figure 26: Four unique up chirp rates with T being between 20ms to 200ms and B = 4kHz (a) and chirp components with instantaneous frequency (b)

This system experimented with various chirp rates. They found the minimum chirp duration to be 20ms and the maximum chirp rate to be 200ms. In practice they most frequently used a chirp duration of 100ms. In addition, each of the up-chirp signals swept from 19kHz to 23kHz, meaning a bandwidth of 4kHz was used to transmit data.

Chapter 4

# DESIGN REQUIREMENTS AND SIMULATIONS

## 4.1 Proposed System

The proposed research for a new kind of IPS system uses ToF to estimate distance between a transmitter and receiver. This topology will use a TDMA scheme to maintain orthogonality between signals. The transmitted signals are unique, linear chirp signals. Each pulse will occupy the same frequency range determined by the bandwidth of the system, which is around 460Hz, and have a duration approaching the impulse response of the system, which is around 3ms.

The instantaneous frequency of the signals is used as a significant measurement tool in the time of flight estimations for this system. The instantaneous frequency measured at the receiver tells which transmitter the signal was sent from, due to each transmitter having a unique signature.

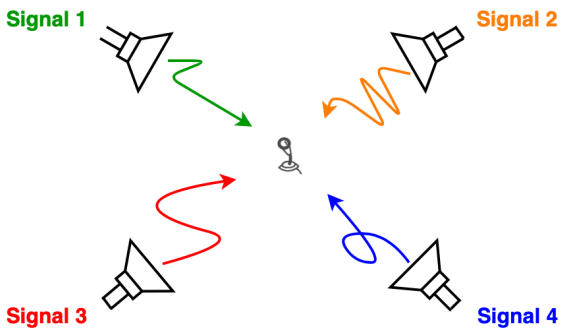


Figure 27: System can identify transmitters as they have distinct signal sweeps and maintain orthogonality using a TDMA scheme

The instantaneous frequency also reveals the time of flight information. This is done by analyzing two signals: the transmitted pulse and the received pulse. In the experimental setup, the transmitted signal can be probed and analyzed simultaneously with signals on the receiver end. However, in a further design of the system, an electromagnetic based mechanism can indicate the initial time of the signal transmission or a frequency at a single point in time.

By extracting the instantaneous frequency of both signals, the precise time of arrival can be determined by comparing when the received signal reaches a particular value. For example, the initial time $t_i$, can be

defined as the point in which the chirp signal to be transmitted reaches 40kHz. The final time $t_f$, can similarly be defined as the point where the chirp reaches 40kHz at the receiver end. The time of flight of the signal can be calculated by:

$$TOF = t_f - t_i \tag{4.1}$$

The instantaneous frequency can provide highly accurate information as to when a particular frequency is received, assuming that the instantaneous frequency remains unaltered. It will be shown later that the instantaneous frequency gets warped due to dispersion effects caused by the bandpass response of the transducers. As a result, the instantaneous frequency plots revealed highly localized deviations that could be detected and measured. This thesis explores the formation of this localized deviation and how it impacts ToF and therefore distance measurements.

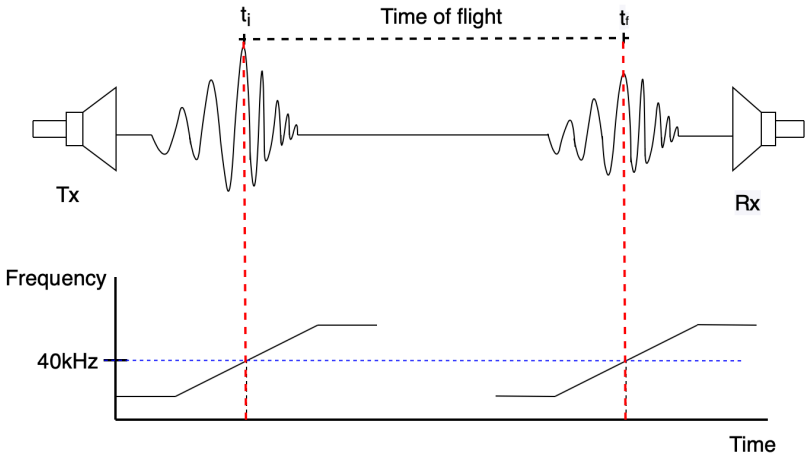


Figure 28: Instantaneous frequency provides time of flight information by measuring time it takes for one frequency to travel from the transmitter to the receiver

## 4.2 Chirp Signal Generation and Synchronization

Four unique chirp signals are used in this system with four transducers to transmit each one. By having a unique sweeping signature, each transmitter can be identified. The four unique signals are made up of a combination of two sweeps: linearly sweeping up and linearly sweeping down. Sweeping up and sweeping down both represent a binary state. This implies that four unique signal transmissions can be generated from two signal sweep directions. This suggests that more transmitters could be implemented

with more combinations of signal sweeps. The number of transmitters can be calculated as $2^N$, given there are N pulses for a single signal transmission.

The sweeping rate and sweeping range are the same for all signals in this system. A fast sweep rate will have an instantaneous frequency ramp resembling a step transition. In this work, a fast sweep is advantageous because steep transitions are easier to detect. This drives the motivation to use a very fast sweeping rate. The sweeping patterns are shown in Table 1. Each of the signals are generated in MATLAB and example code can be found in Appendix A.

Synchronization is necessary in a wireless system because it allows for successful communication between nodes in a network [44]. In addition, synchronization can be used to determine the location of transmitters. The speed of a moving transmitter can also be found if there is common timing between the transmitters. Synchronization is possible in this system by the use of four transmitters in a 3-D space. This concept is used in several other positioning systems including GPS. The receiver can essentially localize itself in an N dimensional space given that there are at least N+1 transmitters. This allows the system to synchronize without having to use an additional communication protocol. This is also a more cost-effective solution.

Table 2: Four unique signal combinations described by their chirping patterns. The corresponding envelopes (not shown) are a pair of pulses

| | |
|---|---|
| Up and Up | Up and Down |
| 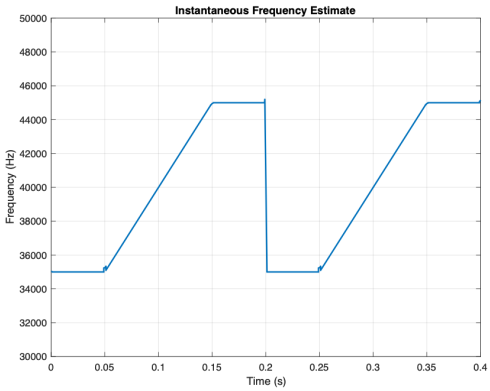 | 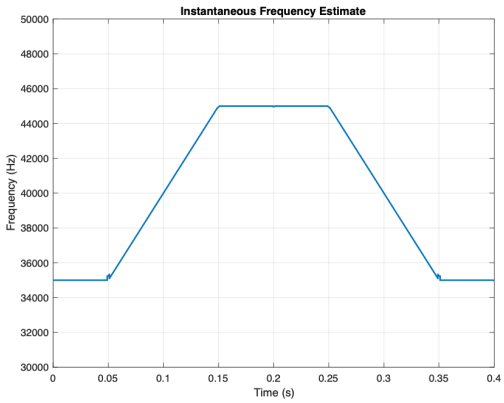 |
| Down and Up | Down and Down |
| 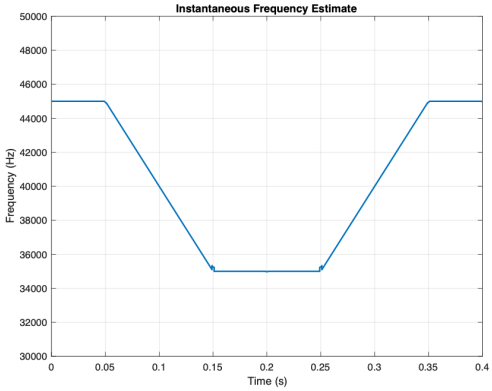 | 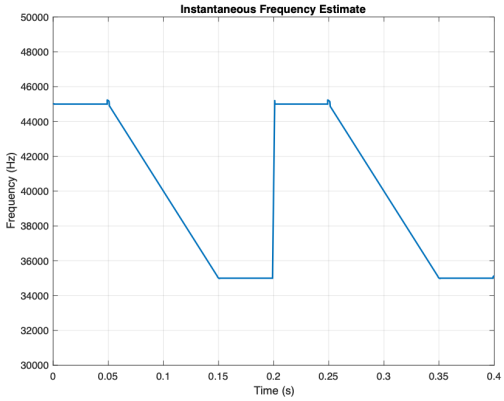 |



4.3 Instantaneous Frequency

In the proposed system, there are two methods used for obtaining instantaneous frequency. In this work, both of these methods post-process the signals in MATLAB. The final expectation would be to implement the processing in a microcontroller to be able to do real time calculations. The first method uses the *instfreq* function, which is a built-in function in MATLAB's Signal Processing Toolbox. In this function, a number of parameters need to be specified including the signal, the sampling rate, and the computation method. In this case, the computation method used is Hilbert, which was discussed in section 2.3. When setting the method to Hilbert, MATLAB estimates the instantaneous frequency using (eq 2.5), where $\phi$ is the phase of the analytic input signal $s(t)$. By definition, an analytic signal $s(t)$ has a spectrum limited to positive frequencies only. This means that with a given real signal in the frequency domain, the analytic signal associated can be determined. Since the definition of the instantaneous frequency in the Hilbert transform is

based on an expression for harmonic motion, it assumes that the signal of interest is a sinusoid. If the instantaneous frequency of a square wave needs to be measured, the Hilbert method is not an option. One example of this is shown in section 2.3 where the envelope of a chirp signal gets clipped. The signal is no longer perfectly sinusoidal for a small duration of the sweep and the Hilbert method does not work.

An additional method is introduced because the instantaneous frequency of square waves is also significant. The hardware on the receiving end produces a square wave with a frequency corresponding to that of the input signal. This will be discussed more in the next chapter. The second method measures instantaneous frequency by measuring the duration of each period, inverting it, and then plotting it versus time. This is done by taking the input signal and converting it to a square wave by passing it through a logical comparator. From there, each period can be measured, and instantaneous frequency can be plotted and observed. The code for this method can be found in appendix B.

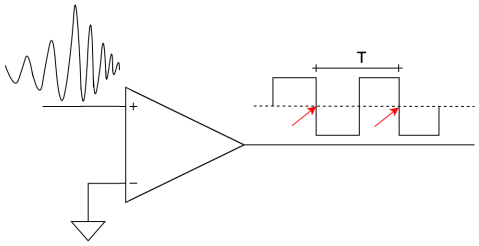


Figure 29: Visual description of zero-crossings method

A comparison of the instantaneous frequency measurements can be seen in figure 30, for a perfect linear up sweep signal. For a perfectly sinusoidal signal, the Hilbert transform is more accurate, and the zero-crossings method curves out slightly in the middle of the sweep.

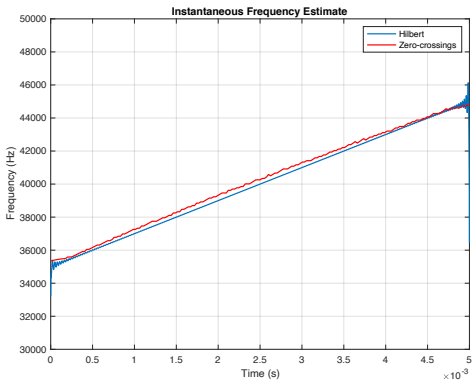


Figure 30: Comparison of instantaneous frequency methods (Hilbert transform and the zero-crossings method) for a perfect up sweep signal

## 4.4 Simulations

### 4.4.1 Ultrasonic Transducers as a Fourth Order Bandpass Filter

Each transducer can be thought of as a second order bandpass filter as shown by the equivalent impedance model discussed in section 1.2. The impedance model implies that the transducers could be represented by a high-Q RLC circuit. Given that each signal goes through two transducers, transmitter and receiver, the overall response can be represented by a fourth order bandpass filter. This model only considers the electrical signal being converted back to an electrical signal, meaning directly from transmitter to receiver. It does not account for the acoustic portion of the transmission that introduces attenuation and delay, which are a function of distance.

The transfer function of a second order bandpass filter can be written as:

$$H_{BP}(s) = \frac{\frac{s}{Q\omega_o}}{(\frac{s}{\omega_o})^2+\frac{s}{Q\omega_o}+1} \tag{4.2}$$

A fourth order bandpass filter can be created by cascading two second order filters. Using a curve fitting algorithm of measuring magnitude response to a fourth order model with two pairs of complex conjugate poles, $Q_1$, $Q_2$, $\omega_1$, and $\omega_2$ were determined [45]. They gave: $Q_1 = 55.94,\ Q_2 = 57.95$, $\omega_1 = 2\pi(40{,}294.8)$, and $\omega_2 = 2\pi(40{,}289.2)$. Using these values, the poles and zeros can be calculated and from there the continuous time transfer function can be derived from MATLAB. The transfer function is then converted from continuous time to discrete time. The MATLAB code for the generation of this filter can be found in appendix C.

The discrete time transfer function of the bandpass filter is:

$$H(z) = \frac{(9.751\times10^{-6})z^3-(9.78\times10^{-6})z^2-(9.693\times10^{-6})z+(9.722\times10^{-6})}{z^4-3.864z^3+5.724z^2-3.847z+0.9911} \tag{4.3}$$

The poles and zeros are acquired from this transfer function and from there the new filter coefficients can be determined. These new filter coefficients are used with MATLAB's built in filter function to serve as the fourth order bandpass filter. The magnitude and phase response of this filter is shown in figure 31.

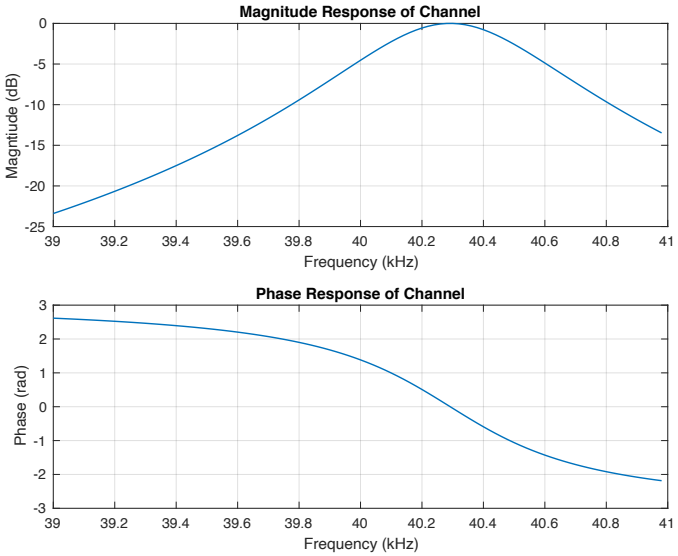


Figure 31: Magnitude and phase response of a fourth order bandpass filter representing the Tx-Rx pair 40TR-12B Tx-Rx

When passing a 100ms linear up-chirp signal from 35kHz-45kHz through the bandpass filter the result is shown in figure 32. The input signal to this bandpass filter was a held constant for 50ms, linearly chirped up for 100ms, and held constant for 50ms. The instantaneous frequency plots shown in figure 33 represent the instantaneous frequency of the signal inside the envelope.

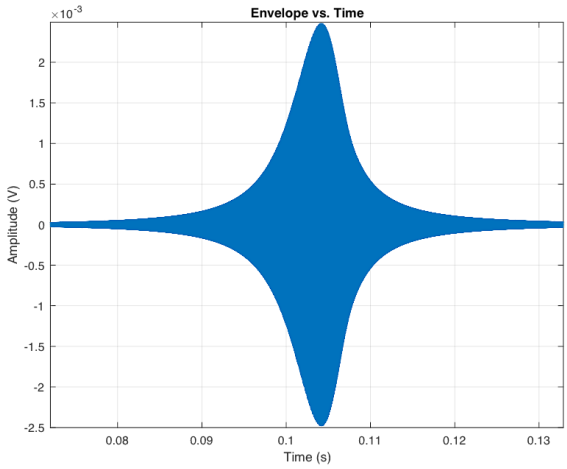


Figure 32: Ideal bandpass response of 100ms linear up-chirp signal from 35kHz to 45kHz

The instantaneous frequency of the up-chirp signal envelope shown in figure 32, was plotted with both methods. Figure 33a shows the instantaneous frequency plot using the Hilbert transform method. Figure 33b shows the instantaneous frequency plot using the zero-crossing method. These two plots reveal that when the signal is a sinusoid, either method works well for extracting the instantaneous frequency. While there are some slight spikes in both plots, these take place outside of the bandwidth of interest and are therefore not problematic.

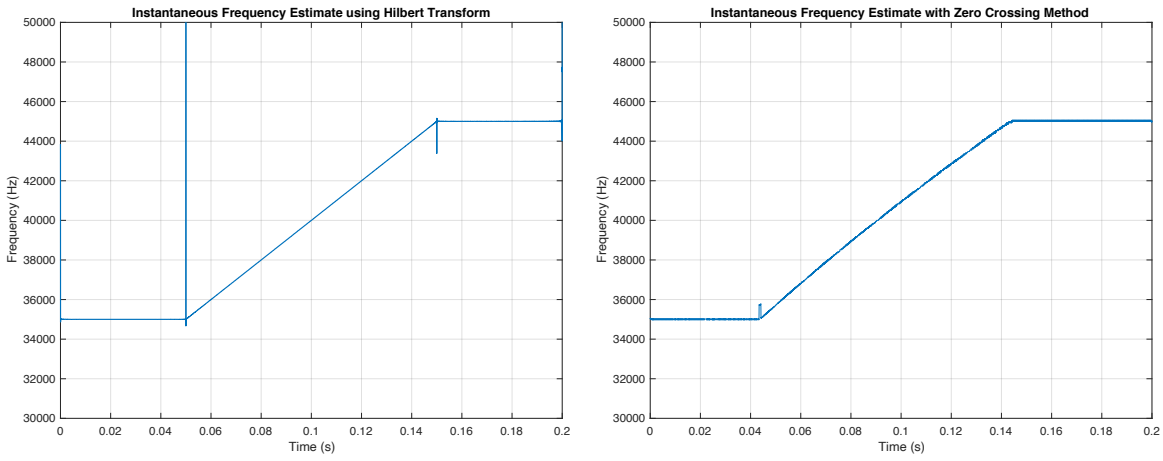


(a) (b)

Figure 33: Instantaneous frequency plots extracted by Hilbert transform method (a) and by measuring time between zero-crossing and inverting method (b)

4.4.2 Chirp Signals: Range and Rate

In this system, all of the chirp signals had a 10kHz sweeping range from 35kHz to 45kHz or vice versa. This sweep range is much larger than the 3dB bandwidth of the transducer pair and most of it falls in the stopband. At both ends of a linear chirp, the signal is held at a constant frequency that is out of the bandwidth of interest. The attenuation of the signal at 35kHz is -47.4dB and the attenuation of the signal at 45kHz is -45dB. The attenuation of these out-of-band signals is significant enough to ensure that this portion of the transmitted signal will not affect orthogonality in the TDMA scheme. In section 1.2, the 3dB bandwidth of the Tx-Rx transducer pair was discussed, which was from 40.06kHz to 40.52kHz. Although the 3dB bandwidth of the transducers is only 460Hz, it is important to note why a larger bandwidth is necessary. The signal needs to have a larger range than the 3dB bandwidth in order to form a narrow pulse

that has out of band frequencies attenuated for enough time to ensure that the pulses are nonoverlapping in time. This ensures orthogonality for a TDMA system.

Chirp signal sweeping rate is a significant parameter that can be optimized by consideration of several factors. Faster chirp rates result in shorter pulses, which benefits localization. The pulse duration is ultimately limited by the duration of the system impulse response. In this work, a "fast" sweep is in reference to sweeping through the bandwidth of the transducers in an amount of time similar to the duration of the impulse response (~3ms).

In figure 34, a 500ms up-chirp signal is shown. This signal has a peak to peak envelope amplitude of $5.05mV_{p\text{-}p}$. Although most signals used in this work were significantly smaller than this 500ms chirp signal, it is important to note that with a long and sturdy signal sweep, this is what the envelope should look like. This ideal pulse envelope traces the magnitude response of the bandpass filter.

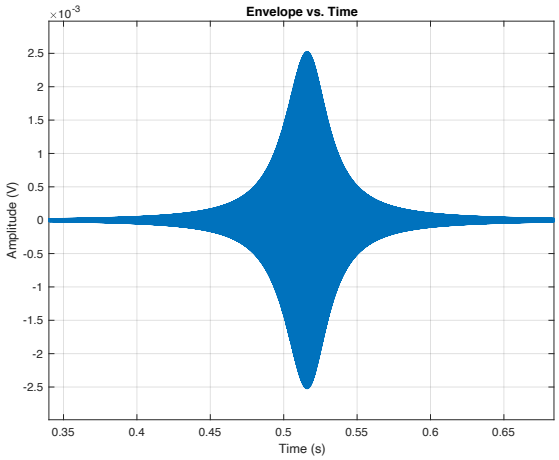


Figure 34: 500ms up-chirp signal sweeping from 35kHz to 45kHz through a fourth order bandpass filter

The FFT of these pulse signals can indicate bandwidth by determining the frequencies at which the magnitude is $\frac{1}{\sqrt{2}}$ of the normalized FFT. For the 500ms up chirp signal from 35kHz to 45kHz, the FFT of the transmitted signal had 3dB frequencies from 35kHz to 45kHz, indicating a 3dB bandwidth of 10kHz. The FFT of the received signal shows a 3dB frequency from 40.07kHz to 40.53kHz indicating an approximate 3dB bandwidth of 460Hz. This is the expected 3dB bandwidth, since it is also the 3dB bandwidth of the transmitters.

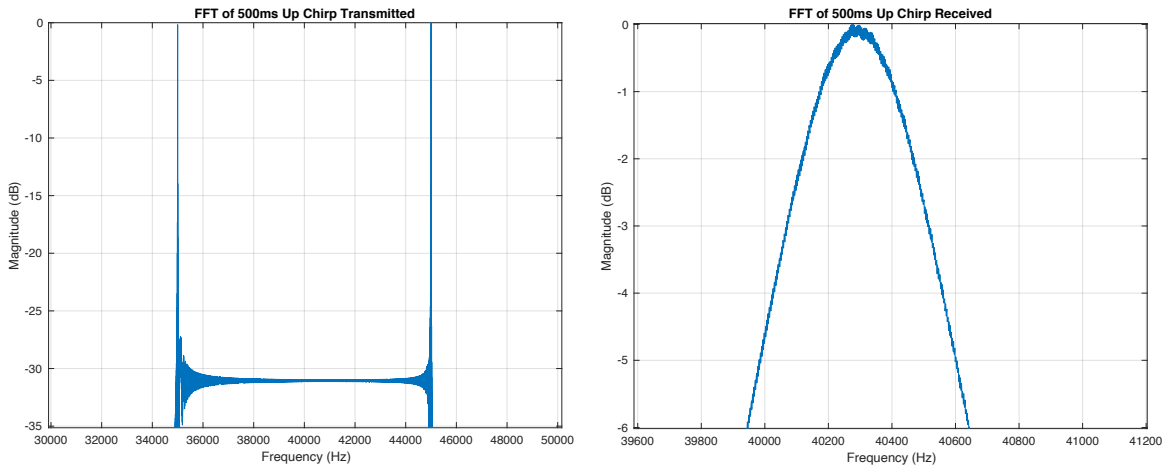


(a) (b)

Figure 35: FFT of 500ms up chirp signal sweeping from 35kHz to 45kHz transmitted (a) and received (b)

The instantaneous frequency of the received pulse was calculated and plotted using both methods and can be seen in figure 36a. A small deviation can be observed in the middle of the sweep in the instantaneous frequency plots. This deviation is extracted and shown in figure 36b. The deviation was approximately 280Hz. It is important to note that the deviation only occurs within the sweep. This will be discussed further in section 4.4.3.

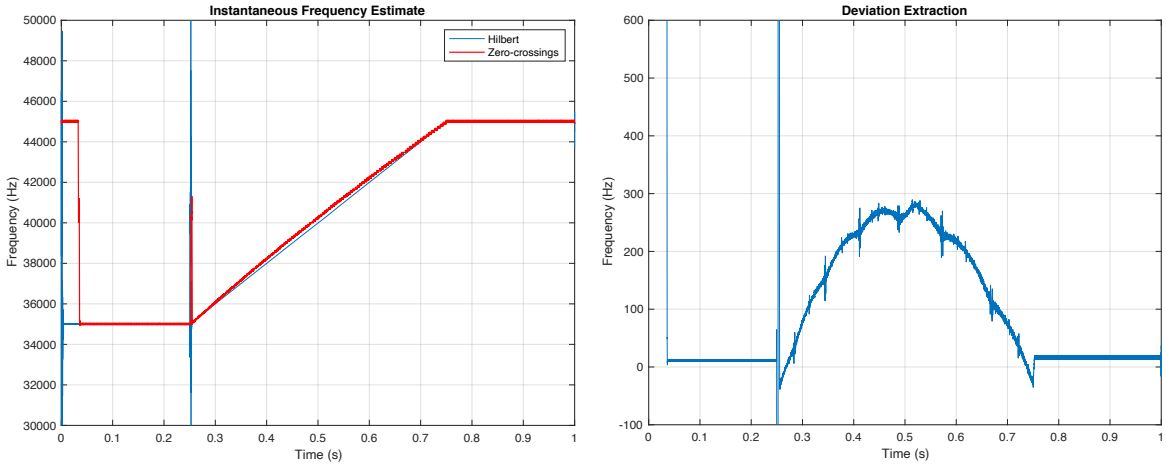


(a) (b)

Figure 36: Instantaneous frequency plot of received 1s signal with 500ms up chirp from 35kHz to 45kHz for Hilbert transform method vs. zero-crossing method (a) and difference extracted (b)

The 500ms down chirp signal was also analyzed. The pulse magnitude was approximately 5.05mV$_{p\text{-}p}$, which is the same as the pulse for the 500ms up chirping case. The envelope shape is also representative of the filter's magnitude response, similar to the up-chirping case.

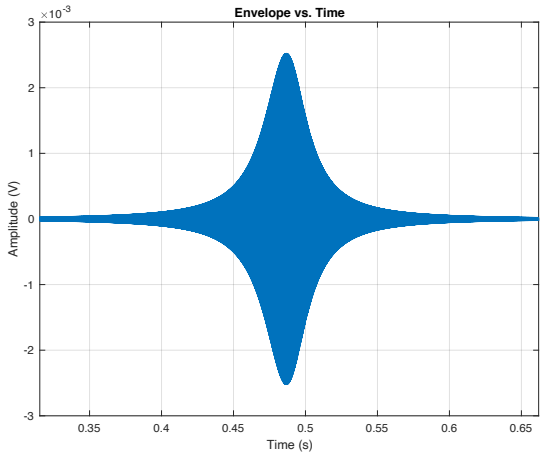


Figure 37: 500ms down chirp signal sweeping from 45kHz to 35kHz through a fourth order bandpass filter

The FFT of both the transmitted and received signal of the 500ms down chirp shows that it matches the 500ms up chirp. The transmitted 3dB frequencies were from 35kHz to 45kHz, resulting in a 3dB bandwidth of 10kHz. The received 3dB frequencies were from 40.07kHz to 40.53kHz, resulting in a 3dB bandwidth of 460Hz. This aligns with expectations as it also matches the 3dB bandwidth of the filter.

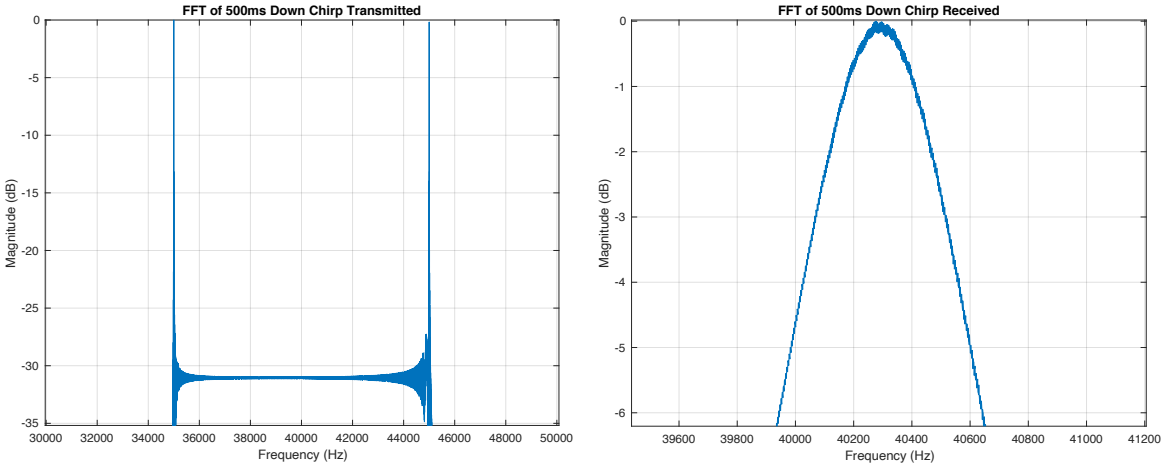


(a) (b)

Figure 38: FFT of 500ms down chirp signal sweeping from 45kHz to 35kHz transmitted (a) and received (b)

The instantaneous frequency plots similarly indicated a deviation in frequency. The overall deviation was around 283 Hz, very similar to what was seen in the 500ms up chirp case.

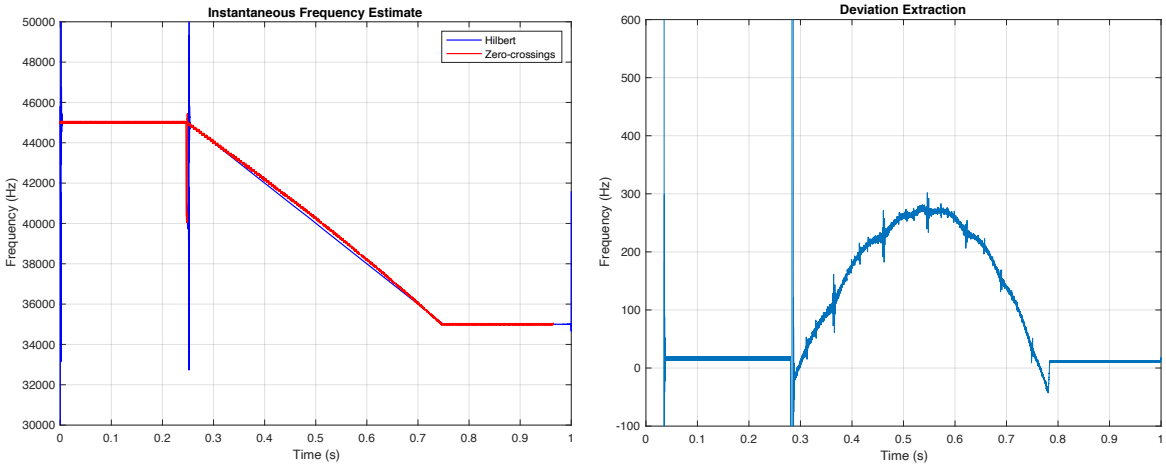


(a) (b)

Figure 39: Instantaneous frequency plot of received 1s signal with 500ms down chirp from 45kHz to 35kHz for Hilbert transform vs. Zero-crossing method (a) and difference extracted (b)

Figure 40 shows the pulse of a signal sweeping from 35kHz to 45kHz for 100ms, and the envelope magnitude is approximately 4.96mV$_{p\text{-}p}$. The signal magnitude is only used as a rough indicator of signal arrival.

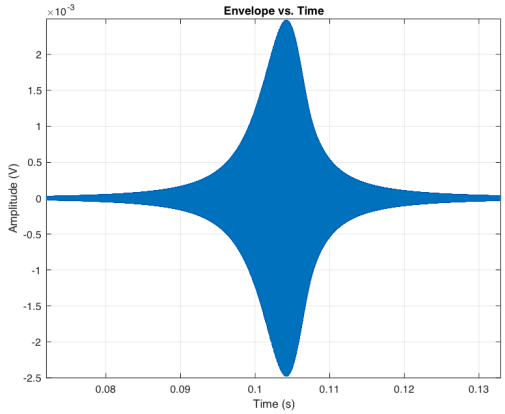


Figure 40: 100ms up chirp signal sweeping from 35kHz to 45kHz through fourth order bandpass filter

The 3dB bandwidth of the 100ms up chirp signal transmitted is 10kHz from the 3dB frequencies being 34.99kHz to 44.99kHz. The 3dB frequencies of the 100ms up chirp signal received is from 40.06kHz

to 40.52kHz. The 3dB bandwidth of the received signal is 460Hz, which is exactly the same as the magnitude response of the fourth order bandpass filter representing the Tx-Rx pair.

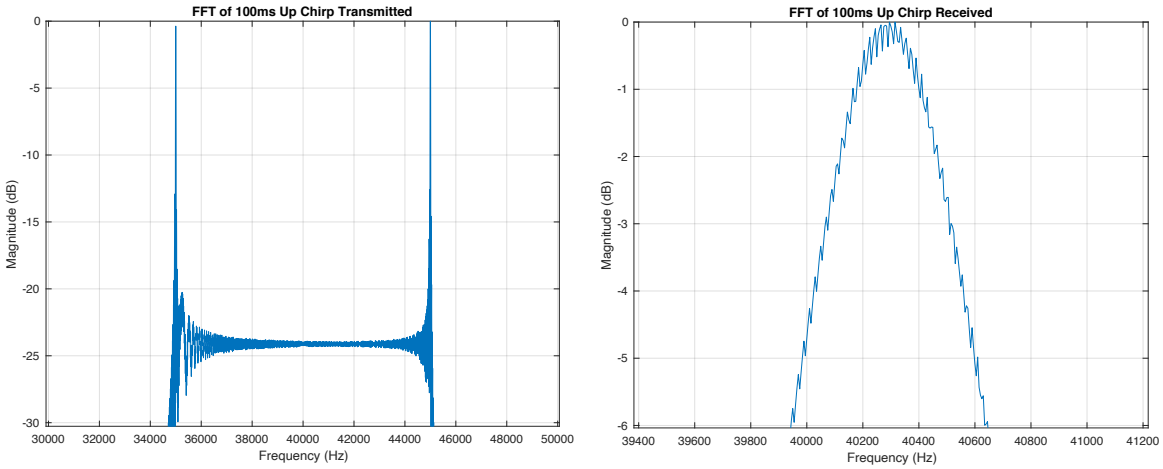


(a) (b)

Figure 41: FFT of 100ms up chirp signal sweeping from 35kHz to 45kHz transmitted (a) and received (b)

The instantaneous frequency plots for the 100ms up chirp from 35kHz to 45kHz are shown in figure 42a. The deviation was extracted and is shown in figure 42b. The deviation shape is similar to what was seen in the 500ms sweeping cases, however the overall deviation is slightly higher as it reaches approximately 308Hz.

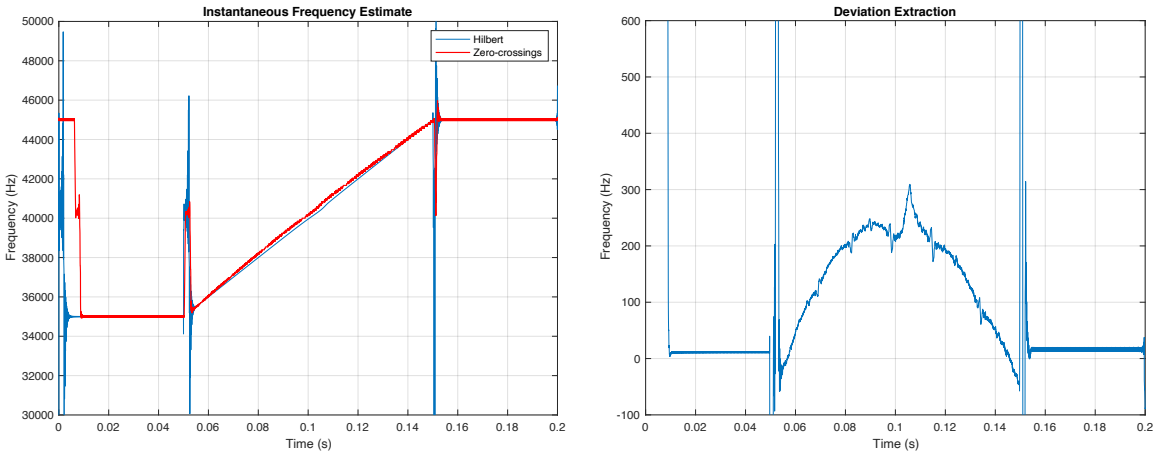


(a) (b)

Figure 42: Instantaneous frequency plot of received 200ms signal with 100ms up chirp from 35kHz to 45kHz for Hilbert transform method vs. Zero-crossing method (a) and zero difference extracted (b)

The 100ms down chirp was very similar to the 100ms up chirp. The envelope magnitude is approximately 4.95mV$_{p\text{-}p}$, which is very close to the is 4.96mV$_{p\text{-}p}$ magnitude of the 100ms up chirp case. The envelope is also representative of the filter's magnitude response. This implies that a 100ms sweep (up or down) is sturdy and not too fast that it would alter the pulse envelope.

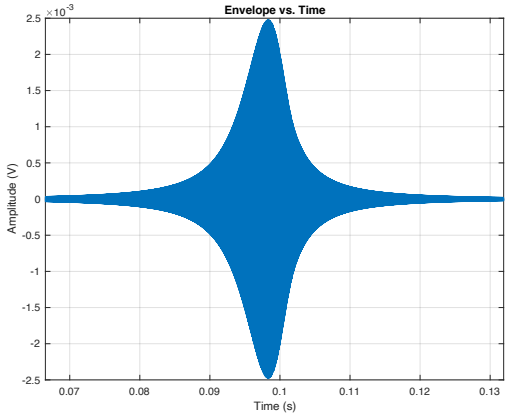


Figure 43: 100ms down chirp sweeping from 45kHz to 35kHz through fourth order bandpass filter

The 3dB frequency of the transmitted signal was from 34.99kHz to 44.99kHz, resulting in a 3dB bandwidth of 10kHz. The 3dB frequencies of the received signal are from 40.05kHz to 40.5kHz. This results in a 3dB bandwidth of approximately 450Hz.

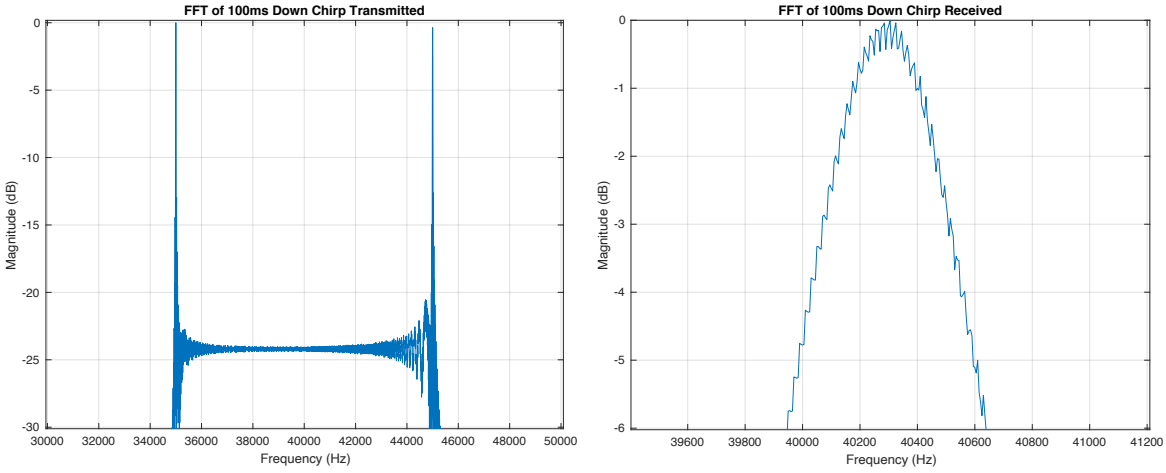


Figure 44: FFT of 100ms down chirp signal sweeping from 45kHz to 35kHz transmitted (a) and received (b)

The instantaneous frequency plot for the 100ms down chirp case is shown in figure 45a. The deviation of the two plots is shown in figure 45b. The maximum deviation is approximately 287 Hz.

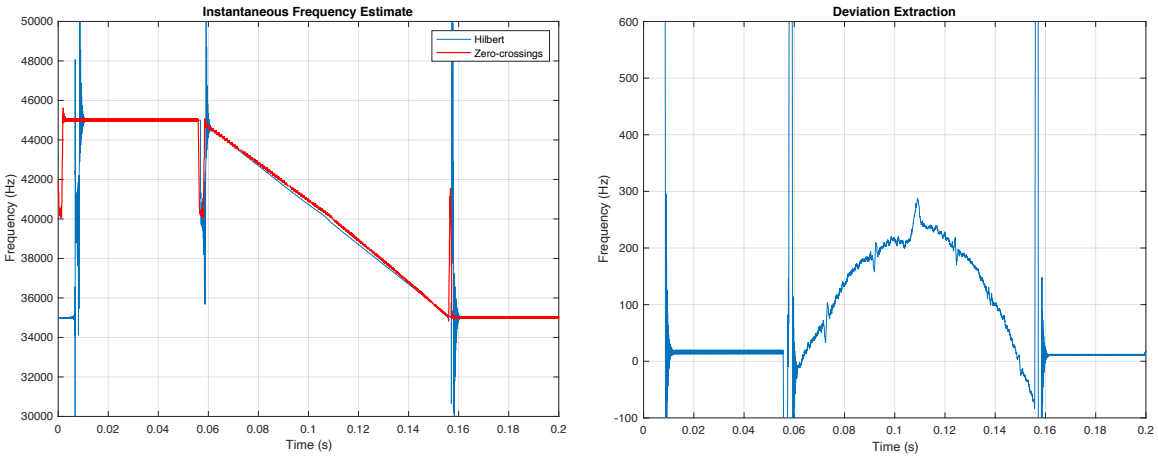


(a) (b)

Figure 45: Instantaneous frequency plot of received 200ms signal with 100ms down chirp from 45kHz to 35kHz for Hilbert transform method vs. Zero-crossings method (a) and deviation extraction (b)

The 100ms sweeps provided sturdy signals that did not alter the envelope shape and were able to provide clear instantaneous frequency data. Another sweeping rate of 25ms was analyzed to see how a more aggressive sweeping rate affects bandwidth and frequency deviation. In this work, 25ms is considered to be a very fast sweep rate since it attempts to cover 10kHz in 25ms. This means it attempts to sweep through 500Hz, close to the bandwidth of the filter in 1.25ms, which is shorter than the duration of the impulse response.

Figure 46 shows an envelope with a signal sweeping up from 35kHz to 45kHz for 25ms and the envelope magnitude is around 4.46m$V_{p\text{-}p}$. Although this is a much faster sweeping rate than the 100ms chirps, the envelope magnitude only decreases by about 10%. This pulse envelope is not the same shape as the 100ms sweep or the magnitude response of the filter. The envelope appears the same at the start of the sweep and gets bumpier on the back end. Although the pulse envelope is affected, this does not imply whether or not the instantaneous frequency inside is affected. With the faster sweep rate, the envelope shape is less defined and wiggles before tapering off. Further discussion on this can be found in Appendix D.

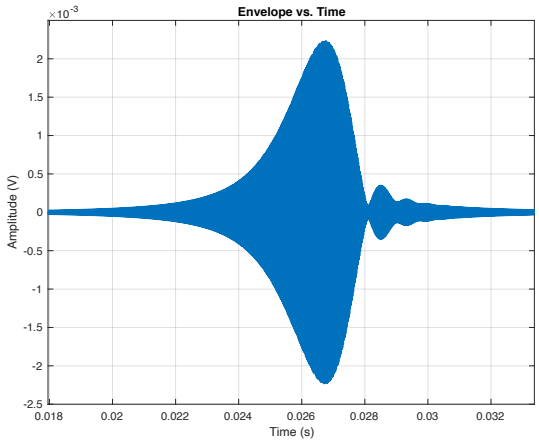


Figure 46: 25ms up chirp signal sweeping from 35kHz to 45kHz through fourth order bandpass filter

The FFT of the 25ms up chirp is shown in figure 47. The transmitted signal has a 3dB bandwidth of 10kHz, with 3dB frequencies from 35kHz to 45kHz. The received signal has a 3dB bandwidth of 440 Hz, with 3dB frequencies from 40.08kHz to 40.52kHz. The 3dB bandwidth of the received signal has decreased compared to the 460Hz from the 100ms up chirp. This indicates that the transducer suppresses more aggressive sweeps.

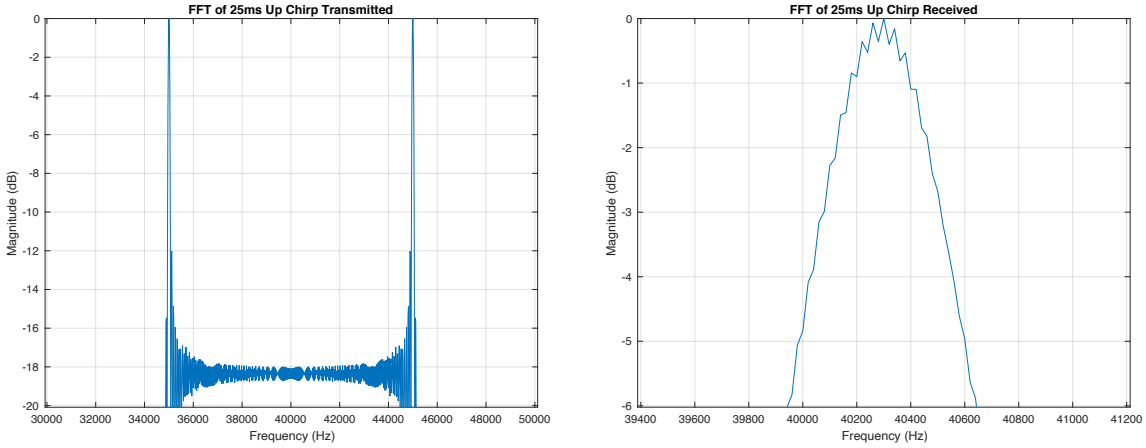


(a) (b)

Figure 47: FFT of 25ms up chirp signal sweeping from 35kHz to 45kHz transmitted (a) and received (b)

The instantaneous frequency plots for the 25ms up chirp are shown in figure 48a. There is a large deviation in the middle of the up-sweeping portion. This deviation is approximately 787Hz. This is a lot higher than the deviation from the 100ms sweeps, which were both around 300Hz. Both methods of

plotting the instantaneous frequency appear to have deviations. The 25ms sweep is unique because of the large spike that occurs in the middle of the deviation.

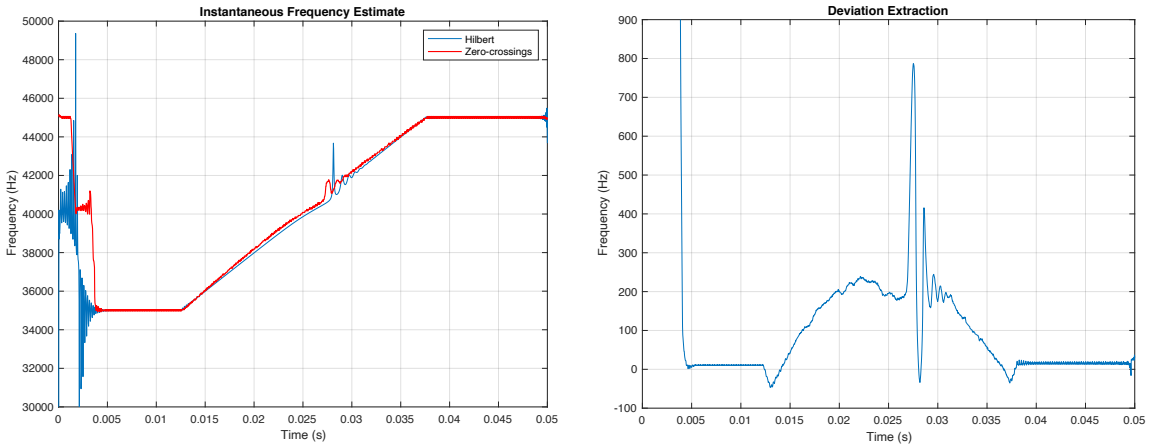


(a) (b)

Figure 48: Instantaneous frequency plot of received 50ms signal with 25ms up chirp from 35kHz to 45kHz for Hilbert transform method vs. zero-crossing method (a) and deviation extraction (b)

The localized spike that takes place in the deviation extraction could potentially be useful for frequency detection. The spike takes place at a point in the pulse where the amplitude is relatively high, meaning that this spike would not be attenuated and could be detected. The red plot shows the instantaneous frequency using the zero-crossings method.

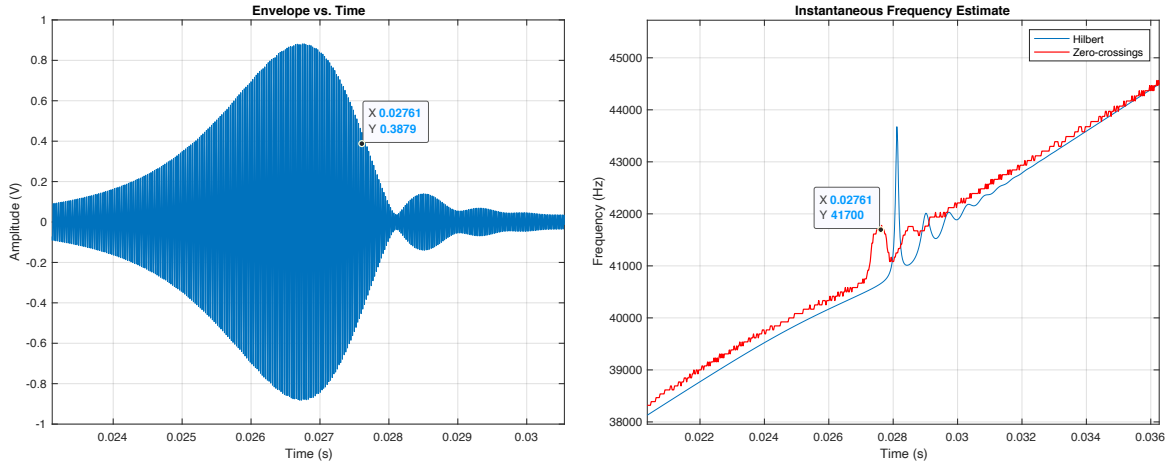


(a) (b)

Figure 49: The marked point in the pulse is where the spike takes place in the instantaneous frequency plot (zero-crossings method) for a 25ms up chirp

The blue spike shown is from the instantaneous frequency using the Hilbert transform. This large spike takes place where the pulse is highly attenuated and is a result of a sharp change in phase. Since this point in the pulse is not in the primary envelope and has a very low magnitude, this spike is not useful for frequency detection.

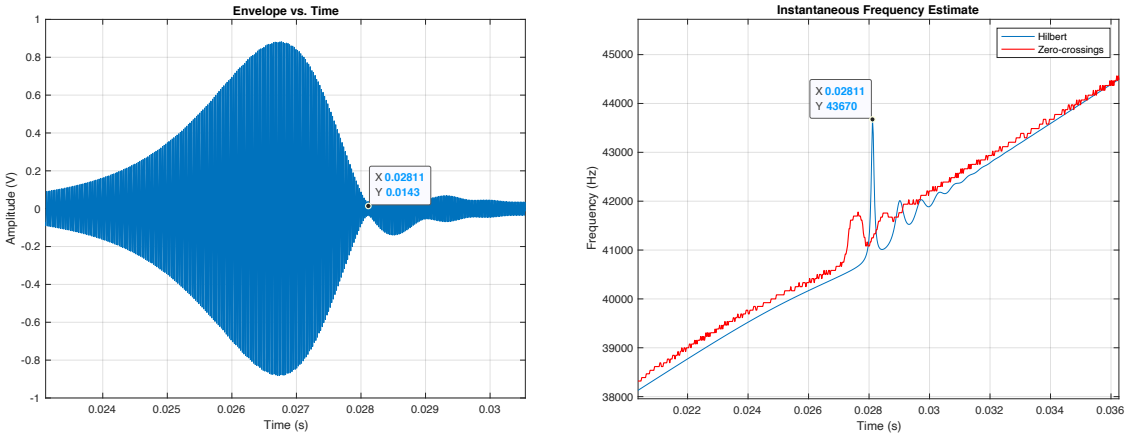


(a) (b)

Figure 50: The marked point in the pulse is where the spike takes place in the instantaneous frequency plot (Hilbert transform) for a 25ms up chirp

Similarly, the 25ms down chirping signal was analyzed. The pulse envelope looks similar to the 25ms up sweeping chirp. This suggests that the pulse envelope is determined by the sweep rate, and not the sweep direction. Both envelopes start out smooth but taper off with smaller pulses toward the end of the sweep. The 25ms down chirp envelope has a magnitude of 4.44mV$_{p\text{-}p}$, which is very similar to the 25ms up chirp.

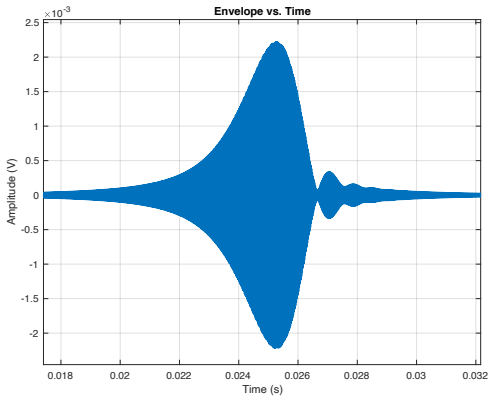


Figure 51: 25ms down chirp signal sweeping from 45kHz to 35kHz through fourth order bandpass filter

The FFT of the transmitted and received 25ms down chirp are shown in figure 52. The transmitted signal has 3dB frequencies of 35kHz and 45kHz, resulting in a 3dB bandwidth of 10kHz. The 3dB frequencies of the received signal are 40.08kHz and 40.52kHz, resulting in a 3dB bandwidth of 440 Hz. This matches what was found in the 25ms up chirping case and confirms that a faster sweeping rate result in a narrower 3dB bandwidth.

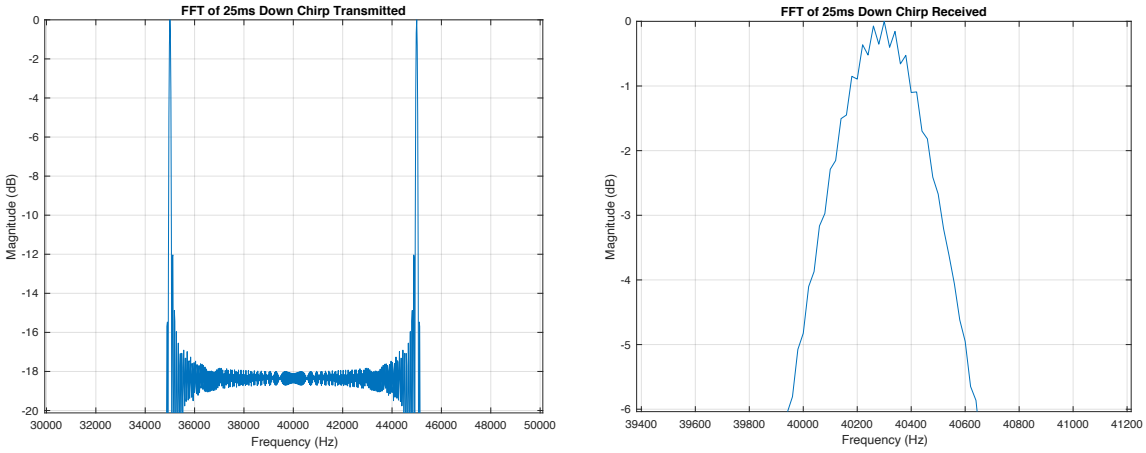


(a) (b)

Figure 52: FFT of 25ms down chirp signal sweeping from 45kHz to 35kHz transmitted (a) and received (b)

The instantaneous frequency plots for the 25ms down chirp are shown in figure 53a. Similar to the 25ms up sweep, there is a large spike in the deviation plot. This maximum point in the deviation is approximately 844Hz. The envelope in figure 55a indicates that this is likely not measurable in practice.

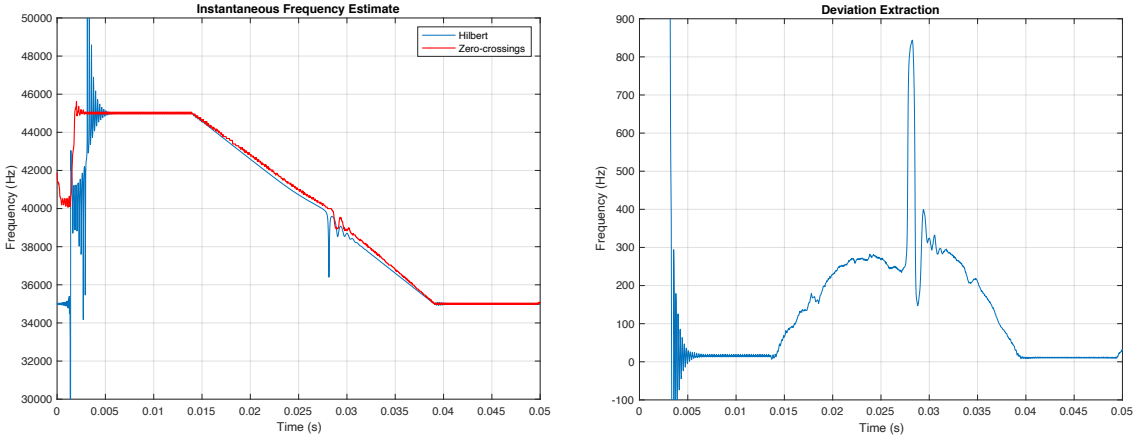


(a) (b)

Figure 53: Instantaneous frequency plot of received 50ms signal with 25ms down chirp from 45kHz to 35kHz for Hilbert transform method vs zero-crossing method (a) and deviation extraction (b)

The localized spike from the zero-crossings method for the 25ms down sweep takes place where the pulse is highly attenuated. This spike is not useful for frequency detection.

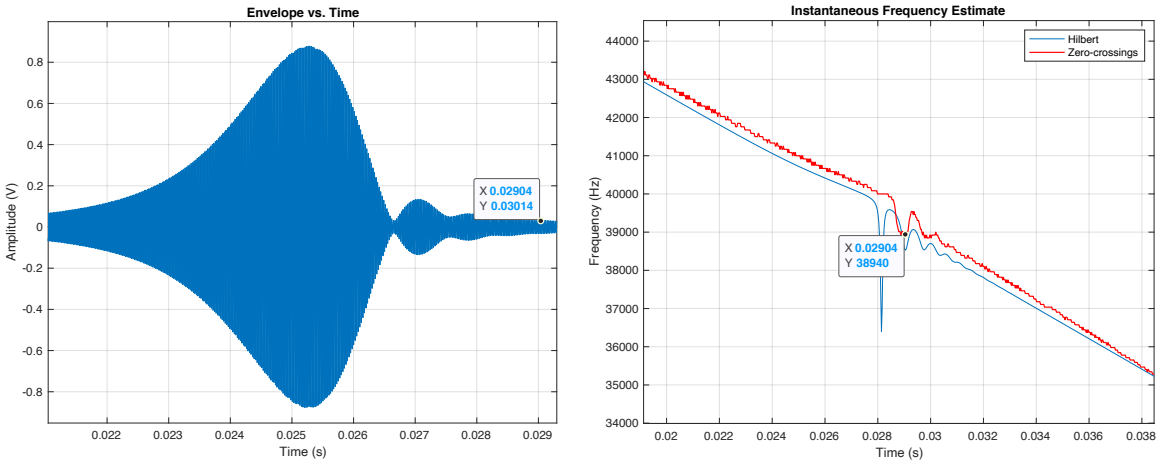


(a) (b)

Figure 54: The marked point in the pulse is where the spike takes place in the instantaneous frequency plot (zero-crossings method) for a 25ms down chirp

Similarly, the spike from the Hilbert transform takes place where the pulse is very small. Since it is outside of the main envelope, this spike is not useful for frequency detection.

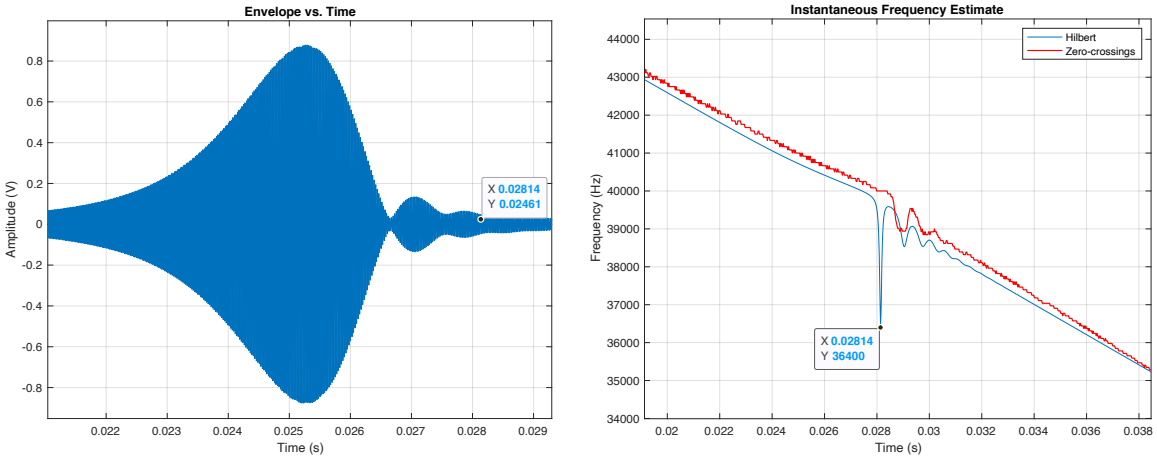


(a) (b)

Figure 55: The marked point in the pulse is where the spike takes place in the instantaneous frequency plot (Hilbert transform) for a 25ms down chirp

When comparing the FFT of the 100ms chirps to the FFT of the 25ms chirps, it becomes evident that the faster the sweep, the narrower the bandwidth. The 3dB bandwidth of the 25ms up chirp FFT is approximately 440Hz. This is smaller than the expected 3dB bandwidth of the Tx-Rx pair of 460Hz and

does not match the bandwidth of the 100ms up chirp. The FFT was also performed on both the 100ms down chirp as well as the 25ms down chirp. These bandwidths are similar to what was seen in the up-chirping cases, meaning that the sweep direction does not have an impact on the bandwidth.

Linear down chirp signals behave similarly to linear up chirp signals of the same rate. The pulse envelope will look approximately the same for the same sweep rates. Similar to the up sweeps of the same rates, the 100ms down chirp is a well-defined envelope that agrees with the magnitude response of the filter. In contrast, the 25ms down chirp is not as clearly defined and has a lower signal magnitude.

### 4.4.3 Artefacts in Instantaneous Frequency Plots

When passing a linear chirp signal into a fourth order bandpass filter in MATLAB, there are some issues that become apparent when analyzing the instantaneous frequency plots. In the instantaneous frequency plots, there are noticeable spikes at the edges of where the constant frequencies meet the linear chirp. While these spikes are very apparent, they are not problematic. These spikes are a result of discontinuities when the constant frequency signals are joined with the chirp signal. This is insignificant because they correspond to frequencies that fall in the stopband. In practice, they will not be observable because the envelope of the pulse is small there and likely corrupted by noise. The most significant parameter for measuring time of flight is the instantaneous frequency of a particular value, for example the center frequency of 40kHz. As long as the instantaneous frequency of the chirp is maintained, the time of flight can be calculated.

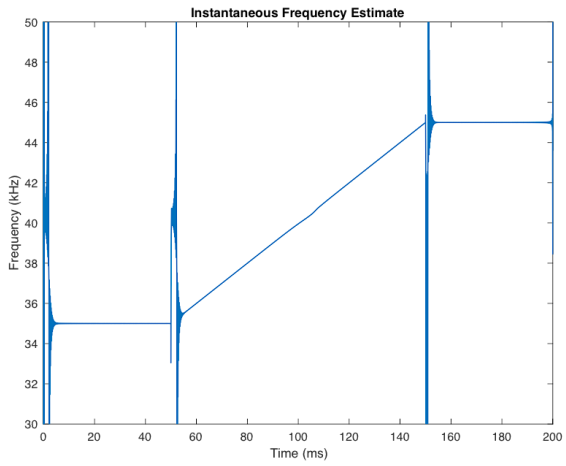


Figure 56: Instantaneous frequency (Hilbert transform) of linear chirp signal passed through a bandpass filter

The issues in the instantaneous frequency plots occur in the middle of the signal. When looking closely at the instantaneous frequency plots, a small 'kink' or deviation can be observed in the middle of the sweep. The abnormality could be observed in up sweeps and down sweeps of different rates. In figure 57, the deviations of the 100ms sweeps and 75ms sweeps are being compared. The instantaneous frequency of these plots were all generated using the Hilbert transform. The deviations were extracted by linear curve fitting and subtracting the difference from the line and the instantaneous frequency. Both plots reveal that the deviations look identical for each sweeping rate. However, they differ from each other in absolute deviation. The 100ms sweeps have an approximate frequency deviation of 88Hz, and the 75ms sweeps have an approximate deviation of 120Hz. In the 100ms sweeps, a frequency deviation of 88Hz means the system would be misidentifying the 40,000Hz as 39,912Hz or 40,088Hz.

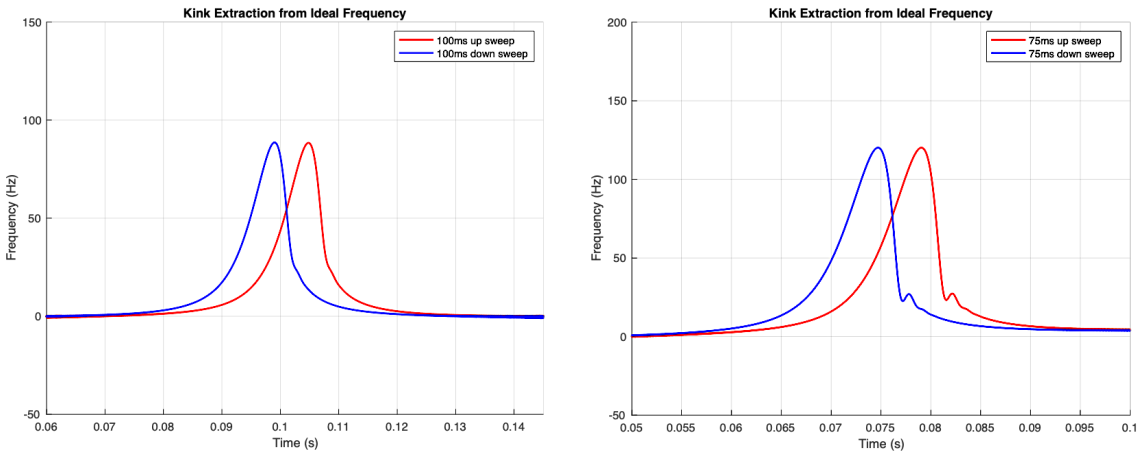


(a) (b)

Figure 57: Deviation extracted from instantaneous frequency plots of 100ms (a) and 75ms (b)

One way to quantify this deviation is as a timing error. Timing error can be defined as frequency error divided by the sweep rate. In the case of the 100ms sweeps, the frequency error is 88Hz and the sweep rate is 100Hz per 1ms. The calculation for the sweep rate for a 100ms sweep is shown below.

$$sweep\ rate = \frac{sweep\ range}{sweep\ duration} = \frac{45kHz - 35kHz}{100ms} = 100\,\frac{Hz}{ms} \tag{4.4}$$

Therefore, the timing error for a 100ms sweep is:

$$timing\ error = \frac{frequency\ error}{sweep\ rate} = \frac{88Hz}{100\frac{Hz}{ms}} = 0.88ms \tag{4.5}$$

A faster sweep would be one solution for reducing the timing error. However, increasing the sweeping rate also increases the frequency error. This can be further shown when calculating the timing

error for the 75ms, which goes up to 0.9ms. However, the error slightly decreases to 0.89ms for a 50ms sweep.

A 25ms sweep was also analyzed to see if it could possibly minimize the error. These sweeps, shown in figure 58, had a much larger frequency deviation of close to 3kHz. This leads to a timing error of 7.5ms, which is far greater than the previous sweeps had. Despite this, since the spikes take place where the pulse magnitude is low, these errors will not have an effect on the system.

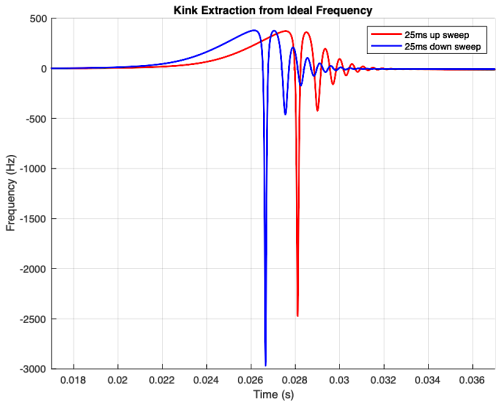


Figure 58: Deviation extracted from instantaneous frequency plot of 25ms sweeps

These deviations in the middle of the instantaneous frequency plots can be attributed to the nonlinear phase response of the transducer pair. To show this, an all pass filter with the same phase response of the fourth order bandpass representing the transducer pair was constructed. The magnitude and phase response of the bandpass filter compared to the all pass filter is shown in figure 59.

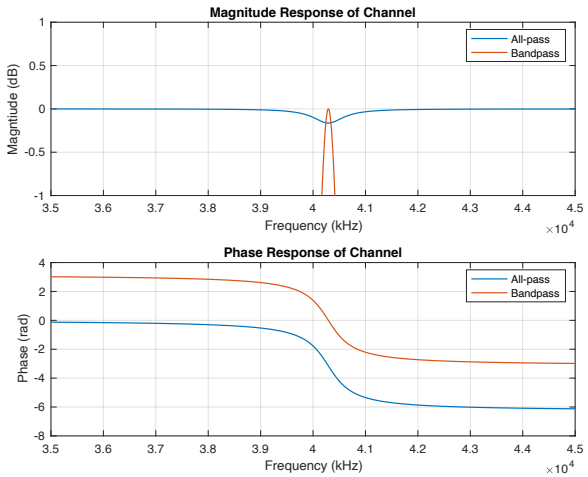


Figure 59: Magnitude and phase response of the fourth order bandpass filter representing the 40TR-12B Tx-Rx and an all pass filter with the same phase response

A 25ms up chirp signal was passed through this all pass filter and the instantaneous frequency was plotted using the Hilbert and zero-crossings method. The plot is shown in figure 60a. Additionally, the frequency deviation was extracted between these two frequency measurements. The shape resembles what was observed for up and down sweeps of different durations shown in section 4.4.2. These plots indicate that this artefact is a result of the nonlinear phase.

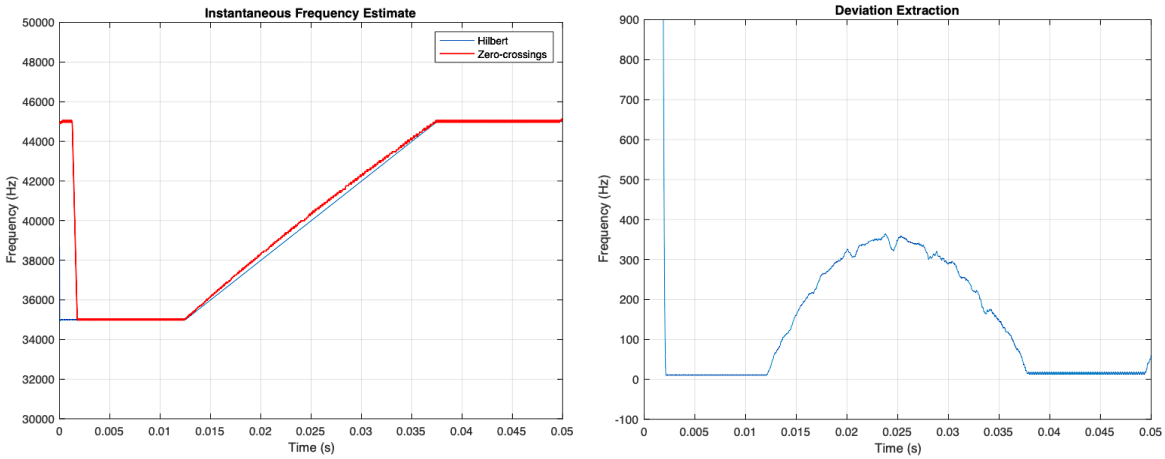


(a) (b)

Figure 60: Instantaneous frequency plot of received signal through an all pass filter with 25ms up chirp from 35kHz to 55kHz for Hilbert transform method vs zero-crossing method (a) and deviation extraction (b)

All of the instantaneous frequency plots generated using the Hilbert method show a slight frequency deviation at some point in the linear frequency sweep, regardless of the rate or if it was sweeping up or down. These deviations are a result of the non-linear phase response of the filter. When sweeping at a more aggressive rate (25ms) large spikes took place within these frequency deviations. Although at first these spikes were considered to be errors, these narrow kinks become ideal for frequency detection.

In order for the deviation to prove useful, it is important to ensure that they are deterministic, meaning that they are not a function of signal strength and are also unaffected by clipping. It is also necessary for the kinks to be highly localized for accurate detection and precise localization. Lastly, the deviation needs to take place within the pulse where the magnitude is sufficiently large to provide

meaningful signal processing. In figures 50 and 55, the large spikes take place outside the pulse, meaning they are largely attenuated. However, these spikes could be used for frequency detection if they took place within the pulse and had sufficient magnitude.

In order to simulate a spike taking place within the pulse, a new signal was generated. Since we know that the spike occurs as a result of a sudden phase change, a new 50ms up chirp signal was generated by multiplying the sweep by -1 after its instantaneous frequency reached around 40kHz. This signal now has a sudden 180° phase change near the center frequency of the transducers. This could show a spike in the instantaneous frequency occurring near the center of the pulse, where the signal is not largely attenuated.

Figure 61a, shows the point in the envelope where the spike takes place. This is near where the signal magnitude is the largest. This means that the spike can be detected through signal processing accurately since the pulse is not attenuated there. Figure 61b shows the instantaneous frequency for this 50ms up chirp signal with inverted phase at 40kHz.

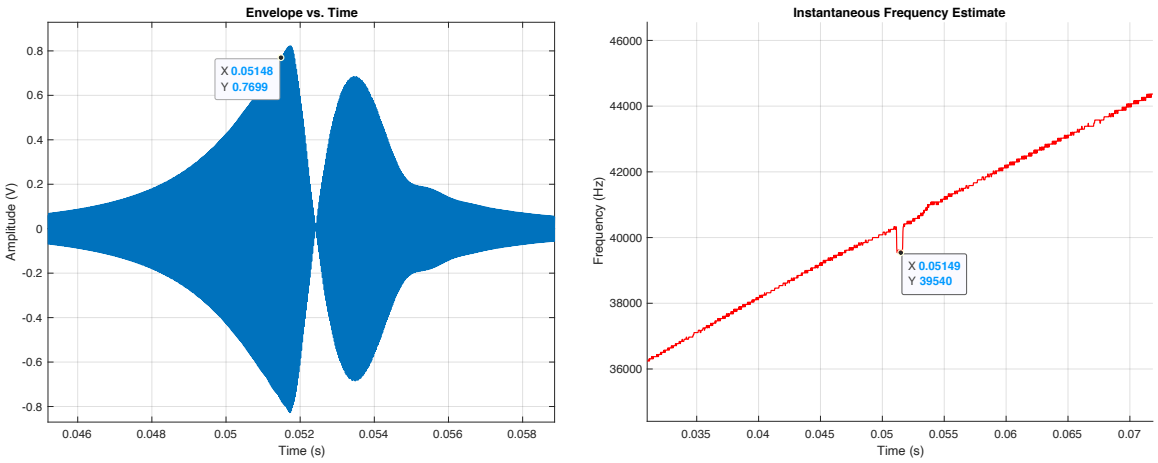


(a) (b)

Figure 61: The marked point in the pulse is where the spike takes place in the instantaneous frequency plot (zero crossings method) for a 50ms down chirp with inverted phase at 40kHz

Chapter 5

# EXPERIMENTAL RESULTS

## 5.1 Receiving Data

Despite the fact that the input signals are sweeping over a 10kHz range, the transducers transmitter and receiver pair have a bandwidth of approximately 460Hz. A received pulse is shown in figure 62. The transmitted signal was a 25ms up chirp from 35kHz to 45kHz. Although the signals lose magnitude outside of the narrow bandwidth, the instantaneous frequency of the signal is maintained.

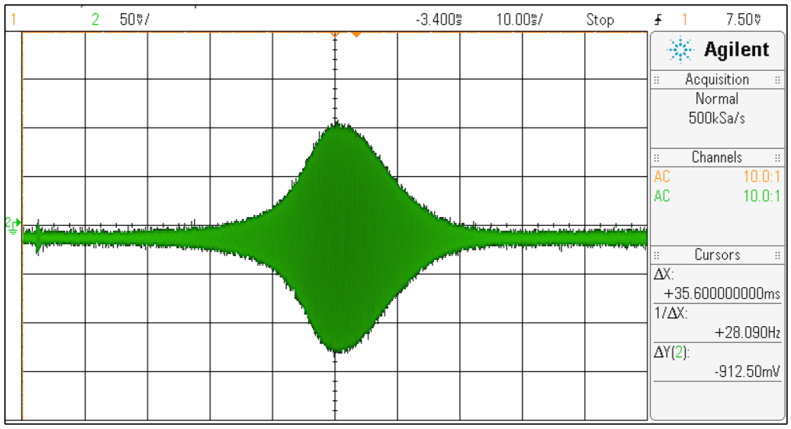


Figure 62: Measured bandpass response of 25ms linear up chirp signal from 35kHz to 45kHz

The instantaneous frequency of the pulse is shown below. The zero-crossings method was used here, and a clear instantaneous frequency plot can be extracted from the measured data.

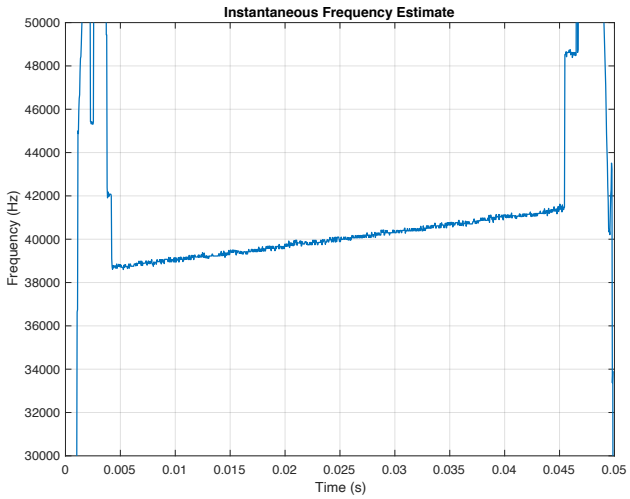


Figure 63: Instantaneous frequency plot of measured pulse with 25ms up chirp from 35kHz to 45kHz

5.2 Hardware Implementation and System Description

In this work, a phase-locked loop (PLL) is used as a signal detection and reception mechanism. A PLL is useful for "locking" on a specific range of frequencies, and then producing a waveform that has a frequency that follows that of the input signal. Because of this, a signal can be easily detected within a frequency range of interest, and the instantaneous frequency of this range can be analyzed.

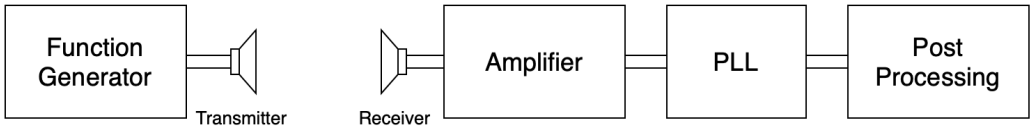


Figure 64: System Block Diagram

The chirp signals were all generated in MATLAB and loaded onto a Rigol DG1062 function generator. From there the signals were sent into the ultrasonic transducer transmitter and received at the transducer receiver. At distances larger than a few inches, the amplitude of the received signal was usually too small to be detected by the PLL circuit without a preamplifier. An LNA 10 low noise amplifier was used in this test system.


Figure 65: LNA10 preamplifier [46]

PLL's are very versatile because they have the ability to extract various features of a signal including instantaneous frequency as well as signal magnitude. The use of a PLL is advantageous because it allows for signals with low magnitude to be detected.

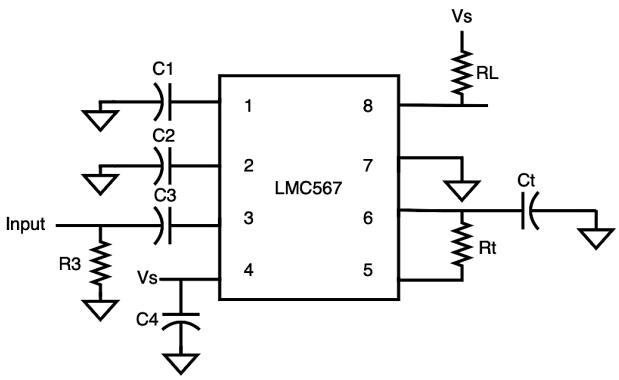


Figure 66: LMC567 application schematic

The LMC567 was the PLL used in this system [47]. There are multiple pins on the LMC567 chip that can provide useful information about the received signal. Pin 1 represents the output filter of the PLL. This pin serves as an amplitude detector as well as a lock detector. When the PLL is locked to the input signal, pin 1 is $\frac{2}{3}V_s$, and when the PLL is not locked, pin 1 is $\frac{7}{9}V_s$. This pin serves as an active pull down since it goes low when the PLL is locked. In input signal with a higher amplitude will cause pin 1 to go more negative.

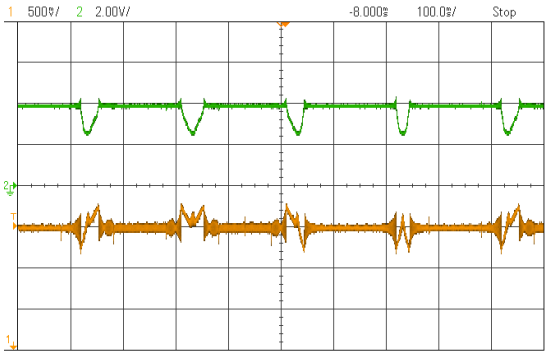


Figure 67: Pin 2 (channel 1 shown in yellow) and Pin 1 (channel 2 shown in green). Pin 1 goes low when the signal is detected and the PLL is locked.

Pin 2 represents the output of the phase detector as well as the control input to the VCO (Vtune). Pin 2 represents the tuning voltage to the VCO, meaning its amplitude is a function of the change in frequency. This is significant because it can serve as a rough estimation for the instantaneous frequency of the input

signal. Not only does it identify where the PLL is locking, it also illustrates the instantaneous frequency shape versus time.

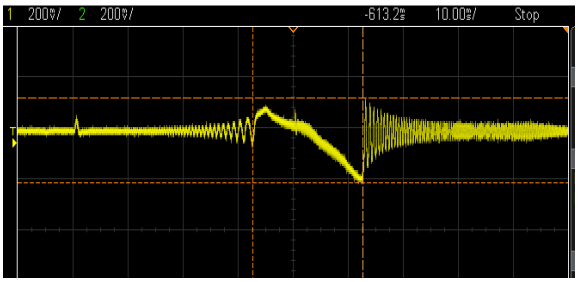


Figure 68: Pin 2 (channel 1 shown in yellow) represents instantaneous frequency

Pin 5 shows the oscillation frequency of the VCO. The VCO is a square wave that has a constant frequency of 80kHz when the PLL is not locked. However, as the input signal changes in frequency, the VCO square wave frequency tracks this. This implies that the VCO frequency is an accurate representation of the input frequency seen by the PLL. Therefore, the instantaneous frequency within the pulse can be accurately measured by determining the instantaneous frequency of the VCO.

## 5.3 The Phase-Locked Loop (PLL)

A deeper analysis of the PLL will show why it is used and what its advantages are. The input signal to the PLL is the received pulse containing a linear chirp from the ultrasonic transducer receiver. The first element in the PLL is the phase detector, which behaves by multiplying the incoming signal with the output of the voltage-controlled oscillator (VCO). The output of the phase detector is a string of pulses with widths varying as a function of the frequency difference between the two signals. This is passed into the loop filter, which is a low pass filter that acts as an integrator. The low pass filter also eliminates high frequency components. The result is a varying signal with time whose amplitude is proportional to the pulse widths. Therefore, the magnitude of this signal is also proportional to the frequency difference between the input signal and the output of the VCO. This signal is noted on figure 69 as $V_{tune}$. $V_{tune}$ is used to adjust the VCO until the output and the input signal have the same frequency and the phase difference remains constant. At this point, the PLL is considered “locked”, hence the name phase-locked loop.

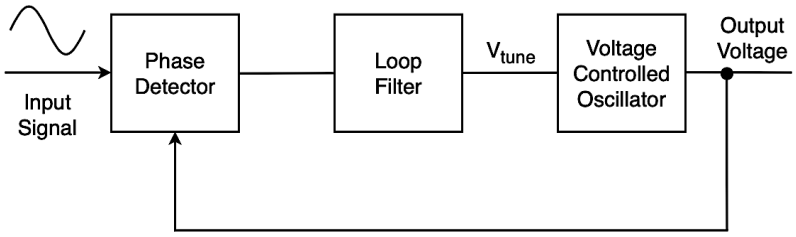

Figure 69: Phase-locked loop

The frequency of the PLL with no input signal is called the free running frequency, fo. The frequency in the LMC567 is set to run at twice the frequency of the input tone. The frequency of interest is 40kHz, which is the center frequency of the ultrasonic transducers. The free running frequency, also known as the oscillation frequency, is set to 80kHz by external components Rt and Ct.

The input signal to the PLL is already bandlimited by the transducer transmitter and receiver pair to around 460Hz. Therefore, the bandwidth of the PLL should be set to some range wider than this narrow frequency range to capture the entire signal. The bandwidth of the LMC567 is set by the oscillation frequency and external component C2. By choosing C2 to be 1nF, the calculated bandwidth of the PLL is approximately 6.4kHz. The capture range of the PLL is the range that the VCO can track the input voltage. The hold range is larger than the capture range and it describes the range of frequencies at which the signals are in phase and out of phase. The overall hold range is from 36.3kHz to 42.5kHz. The measured bandwidth is approximately 6.2kHz, which is close to the calculated 6.4kHz.

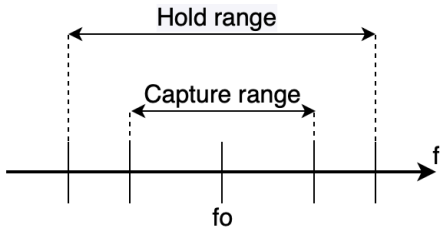

Figure 70: Capture and hold range

5.4 System Setup and Circuitry

The component values used in the LMC567 test circuit are shown in table 3.

Table 3: LMC567 circuit component values

| | |
|---|---|
| **Ct** | 330pF |
| **Rt** | $27k\Omega$ |
| **C4** | 0.1uF |
| **C2** | 1nF |
| **C1** | 10nF |
| **RL** | 270Ω |
| **Pin 3 R** | 47Ω |
| **Pin 3 C** | 10nF |

The test circuit is shown in figure 71. The LMC567 IC was soldered onto a breakout board that easily allowed for circuit prototyping for SOIC-8 packages. The inner few squares represented each pin on the LMC567, while the majority of the board served as a large ground plane.

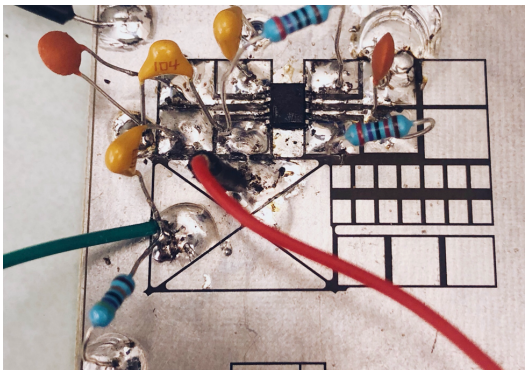

Figure 71: Test circuit built for the LMC567

As mentioned in section 5.2, when in lock, the instantaneous frequency of the VCO matches the frequency of the input signal to the PLL. Therefore, by capturing the VCO data and plotting its instantaneous frequency, it should be representative of the instantaneous frequency received by the PLL. The only difference between the instantaneous frequency of the pulse and the instantaneous frequency of the VCO is that the VCO only follows the instantaneous frequency of the input signal when the PLL is locked. The lock range is smaller than the total sweep range, therefore the sweeping portion of the VCO's

instantaneous frequency will shorter than that of the pulse. Outside of the lock range, the VCO runs at the free running frequency.

Figure 72 shows the VCO square wave probed on channel 2. This signal has a frequency ranging from 35kHz to 45kHz as it follows the input signal sweep. Channel 1 (shown in yellow) represents $V_{tune}$, which also indicates instantaneous frequency. However, this signal's "tuning" level is higher for lower frequencies and lower for higher frequencies. The sweep shown below shows $V_{tune}$ going down, which is really representative of the instantaneous frequency going up. Therefore, this is a linear up chirp signal from 35kHz to 45kHz.

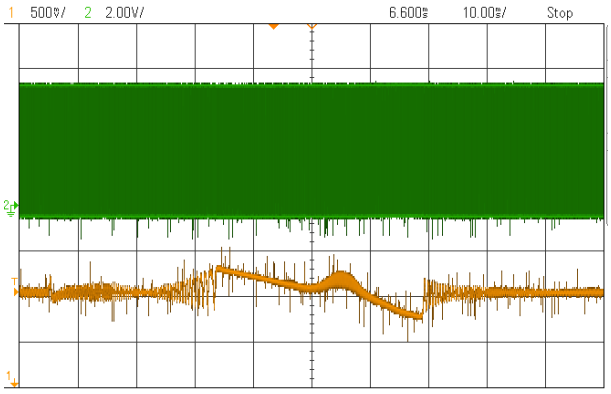


Figure 72: Channel 1 (yellow) represents $V_{tune}$ going down (frequency going up) and channel 2 (green) shows VCO square wave

The data above was post-processed and analyzed in MATLAB. By using the zero-crossings method, the instantaneous frequency of the VCO square wave was plotted and is shown in figure 73. The instantaneous frequency was initially observed as double the expected frequency, as it was centered around 80kHz. This is because the PLL's free running frequency is 80kHz. By altering the zero-crossing method to only account for every other period, the accurate instantaneous frequency plot was observed. This step is necessary to obtain the accurate frequencies that are being received by the PLL. Although the linear sweep is from 35kHz to 45kHz, the plot is only observing a sweep from approximately 38kHz to 41.5kHz. This is because the VCO only tracks the voltage where the PLL is locked, which has a much smaller bandwidth than the total input sweep.

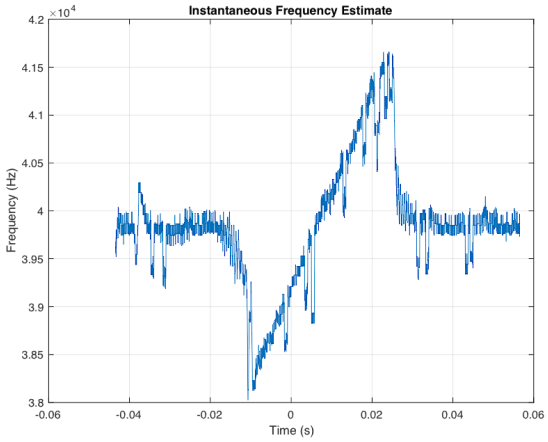


Figure 73: Instantaneous frequency plot of VCO shows linear up chirp signal

Similarly, the VCO square wave and $V_{tune}$ data was acquired for a linear down chirp signal and is shown in figure 74. $V_{tune}$, showing instantaneous frequency is shown as channel 1 (yellow). The VCO square wave, also pin 5, is shown as channel 2 (green). As in the previous example, pin 5 tracks the instantaneous frequency but in an "opposite" manner. The pin has a low signal magnitude when the frequency is high, and a high signal magnitude when the frequency is low. Outside of this sloped magnitude portion, pin 5 is constant when the PLL is not locked.

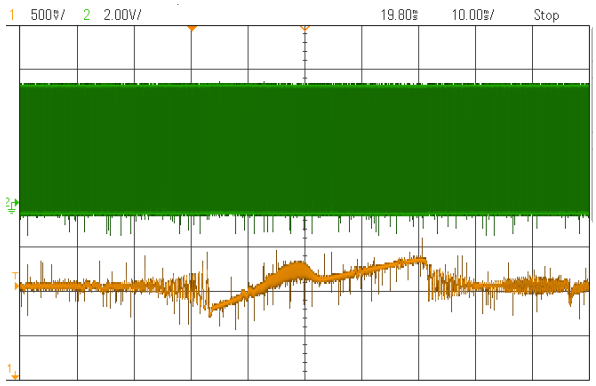


Figure 74: Channel 1 (yellow) represents $V_{tune}$ going up (frequency going down) and channel 2 (green) shows VCO square wave

This data was also post-processed in MATLAB. Using the zero-crossings method, the instantaneous frequency of the VCO square wave was determined. The plot is shown in figure 75, and it is a linear down chirp signal. Outside of the linear sweeping portion, the VCO operates at the free running frequency, which is why the plot shows that it is at 40kHz outside of the sweep. Because of the method

described earlier to half the frequency, this plot indicates that the free running frequency is 40kHz, when it is actually 80kHz.

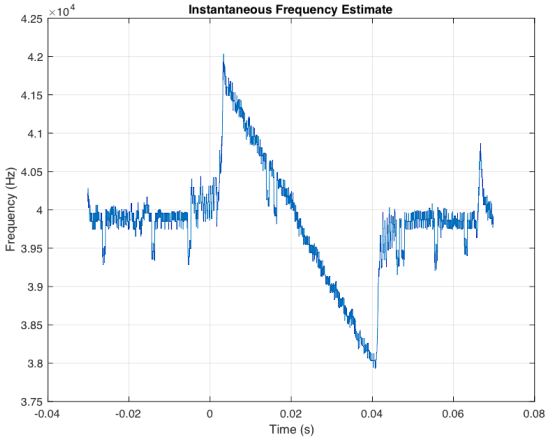


Figure 75: Instantaneous frequency plot of VCO shows linear down chirp signal

Each of the four unique sweeping patterns described in table 2 were tested and their instantaneous frequencies were analyzed. Recall that each of the sweeping patterns contain two sweeps to form four unique sweeping patterns with combinations of up and down chirps. All of the sweeping patterns had sweep durations of 50ms and holding constant frequencies for 50ms on each end. Therefore, the total signal duration containing two sweeps was 200ms. The zero crossings method is used for all of the measurements. The first pattern shown is an up and up chirp.

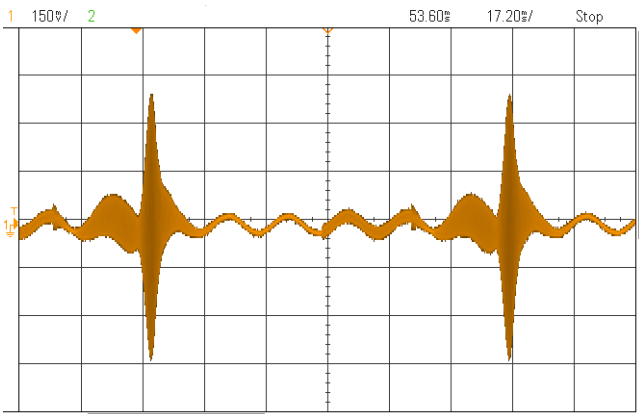


Figure 76: Pulse for 50ms up chirp and 50ms up chirp pattern

The instantaneous frequency of the amplified pulse envelope is shown in figure 77. The instantaneous frequency plot clearly shows the sweeping pattern. In addition, in the middle of the sweeps, small kinks can be observed. In simulation, it was determined that the kinks were a result of the nonlinear phase of the fourth order bandpass model of the transducer transmitter and receiver pair. This plot shows that the kink, or deviation caused by the nonlinear phase of the transducers can be confirmed in measurements.

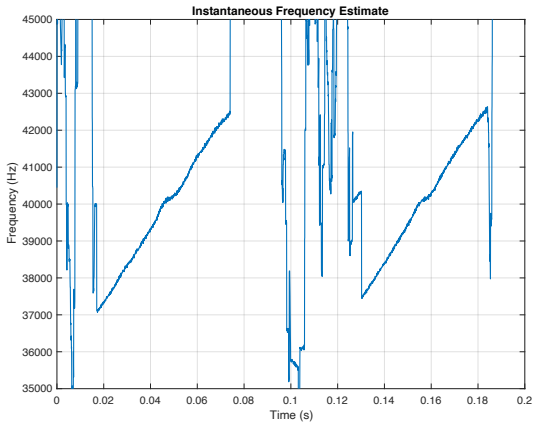


Figure 77: Instantaneous frequency plot of pulse for 50ms up chirp and 50ms up chirp pattern

The instantaneous frequency of the VCO was also analyzed. The plot follows expectations as it clearly has the same sweeping pattern, but the sweeping portion is limited by the PLL's lock range. Outside of the frequency sweep, the VCO runs at the free running frequency of 40kHz.

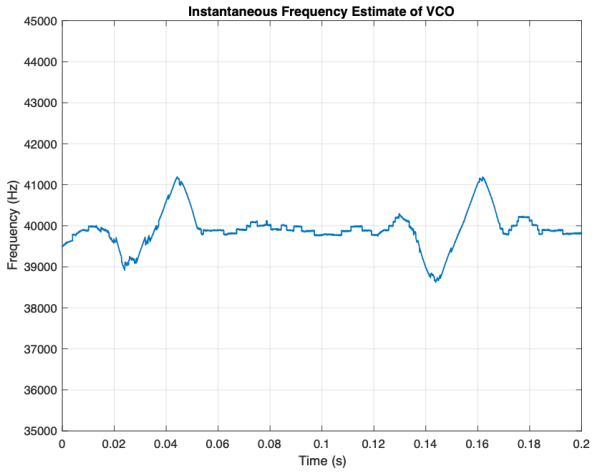


Figure 78: Instantaneous frequency plot of VCO for 50ms up chirp and 50ms up chirp pattern

The pulses from the up and down sweeping pattern is shown in figure 79. Each sweep duration is 50ms. The envelope appears more bulbous at the lower frequency range.

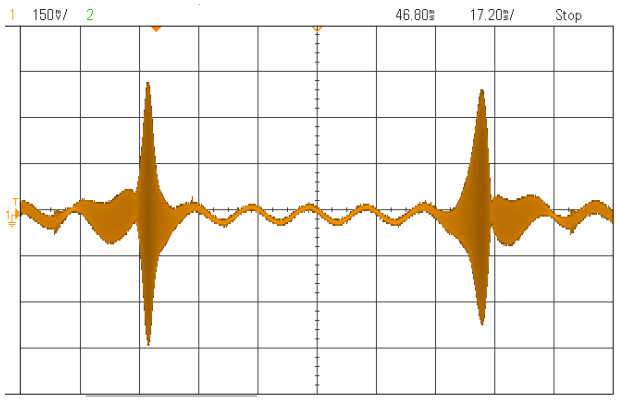


Figure 79: Pulse for 50ms up chirp and 50ms down chirp pattern

The instantaneous frequency of the up and down sweeping pattern is shown in figure 80. Similar to the up and up case, there are artefacts shown in the middle of the sweeps. In the up-sweeping portion, the deviation is small and not easily observable from this plot. In the down sweeping case, there is a much larger deviation in the middle of the sweep.

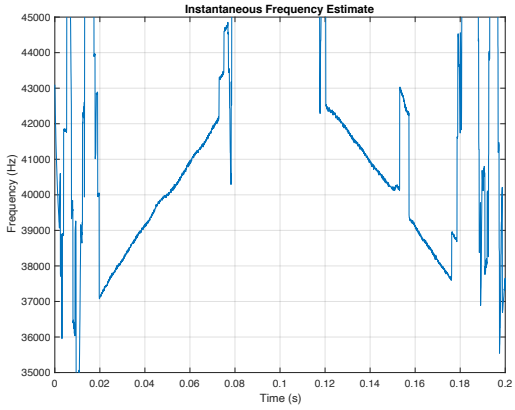


Figure 80: Instantaneous frequency plot of pulse for 50ms up chirp and 50ms down chirp pattern

The instantaneous frequency of the VCO was also observed for this sweeping pattern. The VCO appears to be a lot noisier of a signal than the signal in the envelope. However, the sweeping pattern can still be clearly identified. The large artefact in the down sweeping portion of the pulse's instantaneous frequency is not clearly observed here.

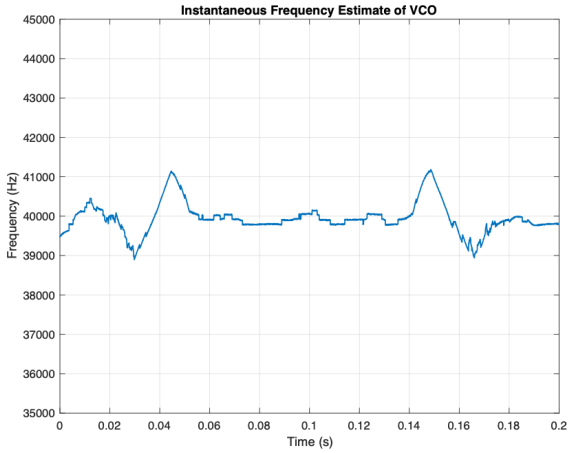


Figure 81: Instantaneous frequency plot of VCO for 50ms up chirp and 50ms down chirp pattern

Similarly, the down and up sweeping pattern was measured. The two pulses from this signal are shown in figure 82. Like in the up and down case, the envelope has a bulbous portion where the lower frequencies take place.

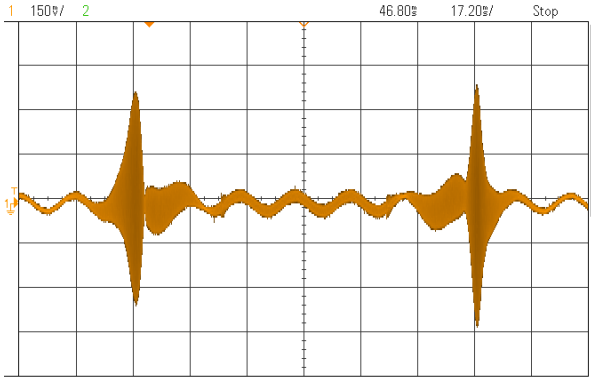


Figure 82: Pulse for 50ms down chirp and 50ms up chirp pattern

The instantaneous frequency of the pulse for down and up sweeping pattern in shown in figure 83. The sweeping pattern is very clear, and the small deviations are noticeable.

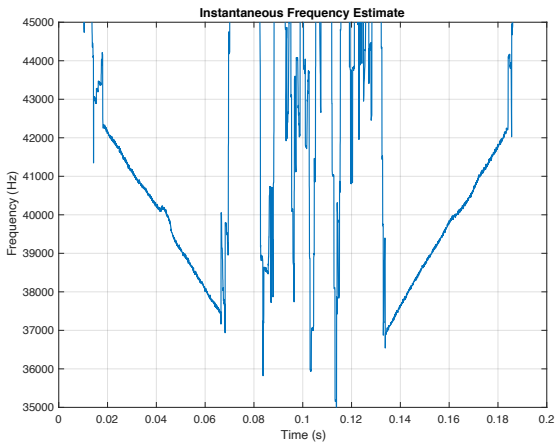


Figure 83: Instantaneous frequency plot of pulse for 50ms down chirp and 50ms up chirp pattern

The instantaneous frequency of the VCO for the down and up pattern is shown in figure 84. Similar to the previous sweeping patterns, the sweep direction can be clearly identified. However, the VCO is noisier and does not necessarily show the deviations.

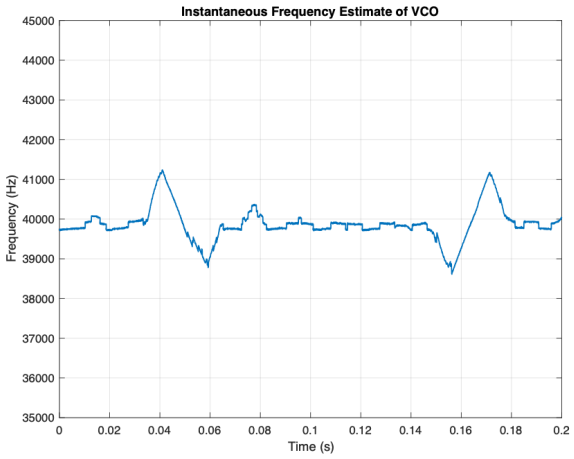


Figure 84: Instantaneous frequency plot of VCO for 50ms down chirp and 50ms up chirp pattern

Lastly, the down and down sweeping pattern was observed. The pulses for these sweeps are shown in figure 85. Similar to the previous pulses, the bulbous part of the pulse takes place at lower frequencies.

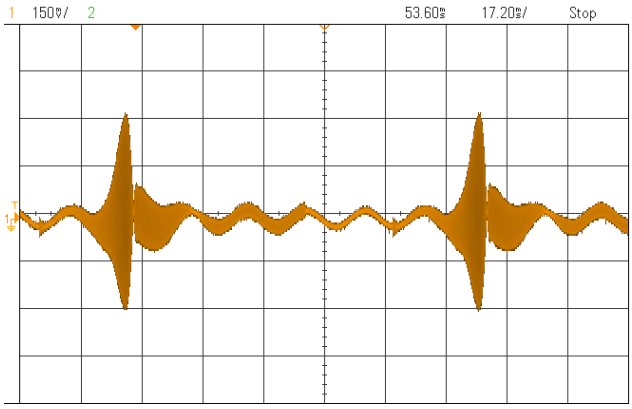


Figure 85: Pulse for 50ms down chirp and 50ms down chirp pattern

The instantaneous frequency for the down and down pattern is shown in figure 86. The sweeping pattern is very clear and both down sweeps are nearly identical. The deviations are also very noticeable and have an identical shape.

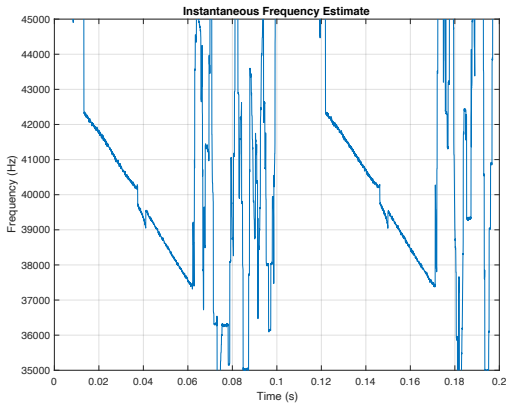


Figure 86: Instantaneous frequency plot of pulse for 50ms down chirp and 50ms down chirp pattern

The instantaneous frequency of the VCO for the down and down sweeping pattern is shown in figure 87. Similar to previous sweeping patterns, the pattern is recognizable, but the signal appears to be noisy. The deviations are not easily identifiable.

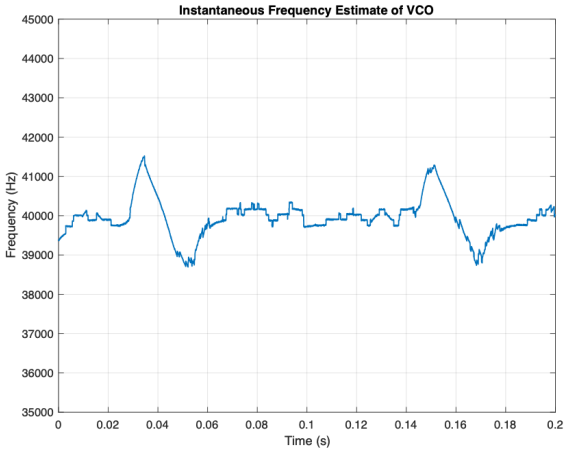


Figure 87: Instantaneous frequency plot of VCO for 50ms down chirp and 50ms down chirp pattern

In section 4.4.3, a 50ms up chirp signal with a 180° phase shift was introduced to show that the deviation or artefact can be created within the pulse envelope and have a large enough magnitude to use for accurate signal processing. The phase discontinuity signal created a split pulse in simulations and indicated that the deviation took place within the pulse envelope.

This phase discontinuity signal was also measured in hardware. The same 50ms up chirp signal was used, with a phase inversion around 40kHz. The measured pulse and corresponding VCO signal are shown below in figure 88.

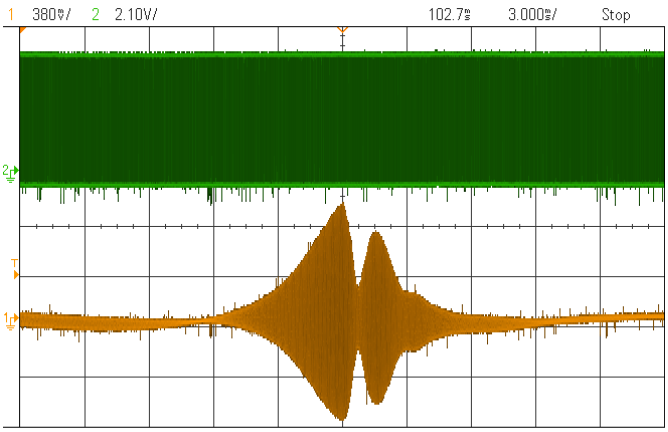


Figure 88: Pulse for 50ms up chirp with phase discontinuity at 40kHz (channel 1 – yellow) and VCO signal (channel 2 – green)

The pulse envelope matches simulations in that it has a split pulse caused by the phase discontinuity. The instantaneous frequency plots were generated for both the pulse as well as the VCO. The instantaneous frequency plot of the pulse shown in figure 89, indicates a large downwards deviation in the middle of the sweep. This spike is large and clearly detectable in the instantaneous frequency plot.

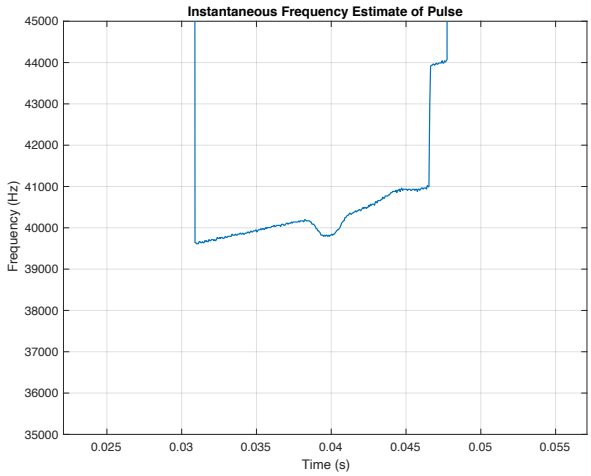


Figure 89: Instantaneous frequency plot of pulse for 50ms up chirp with phase discontinuity at 40kHz

Additionally, the instantaneous frequency of the VCO was measured. The plot shown in figure 90 indicates a similar downwards deviation in the middle of the sweep. This shows that a signal with a phase discontinuity that takes place within the envelope is detectable by observing its instantaneous frequency. This shows promise that deviations caused by nonlinear phase can be useful for frequency detection.

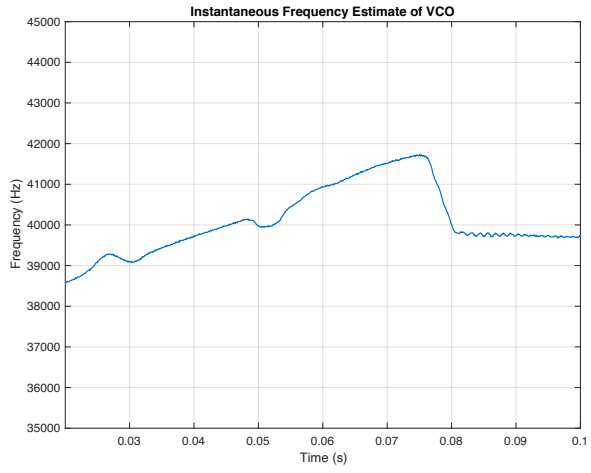


Figure 90: Instantaneous frequency plot of VCO for 50ms up chirp with phase discontinuity at 40kHz

# Chapter 6

# FUTURE WORK

## 6.1. Study the Impact of Noise

In the experimental setup in this system, the transmitter and receiver were separated by distance but with a paper tube connecting them. This was a rough attempt to create a noiseless environment, and also ensure the transmitter and receiver were directly facing each other. In simulations, there was no consideration of noise effects. In a real environment, noise would significantly impact the system as any acoustic signal that can be received by the transducers may interfere with their outputs. Signals that are being transmitted at an increased distance also have a decreased amplitude, and consequently a lower SNR. The PLL helps to reduce noise in some ways as it has a low pass filter that can eliminate some of the high frequency noise components. The first item for future work would be to do a study on the impact of noise on the proposed signaling scheme in both simulations and experimental measurements.

## 6.2. Investigate Intentional Slope Changes at 40kHz

In this work, narrow artefacts have been observed in the middle of the frequency sweeps. These artefacts are a result of an abrupt change in the phase response. The sweeping patterns all swept linearly through the center frequency of 40kHz. However, it would be meaningful to observe other sweeping patterns that have an intentional slope change at 40kHz. There were a few sweeping patterns tested initially that had intentional slope changes but were not further considered. These can be found in Appendix E.

Further investigating the abrupt change at 40kHz could be beneficial if the artefacts are to be used for frequency detection. As mentioned in section 4.4.4., these highly localized spikes could be used for accurate pulse detection. However, these spikes need to take place within the pulse where the signal magnitude is large, unlike in this work, where the large spikes took place where the pulse was largely attenuated. By including fast sweeps with an abrupt change in frequency at 40kHz, these spikes could take place where the pulse magnitude is high, and potentially be a useful tool in frequency detection.

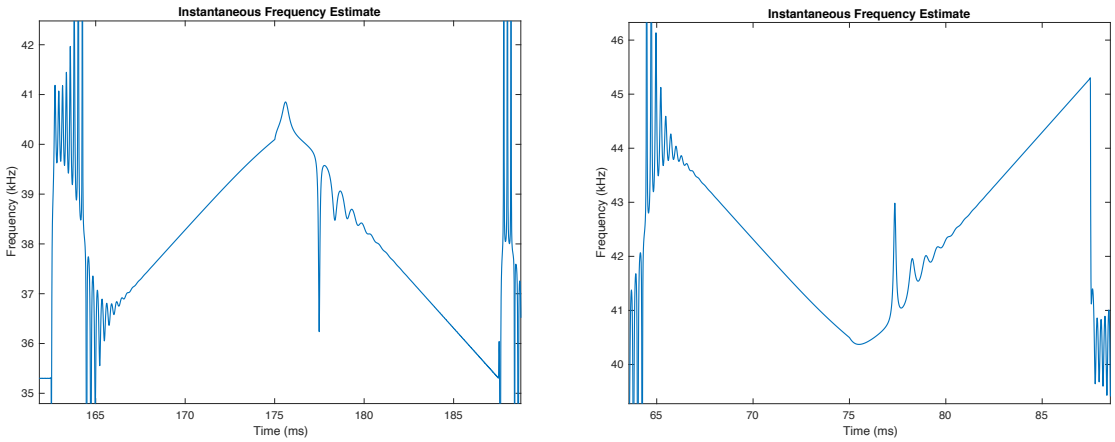


(a) (b)

Figure 91: Sweeping patterns that have abrupt changes at 40kHz could provide useful deviations for frequency detection because the artefacts are likely to take place within the pulse

Figure 92 and figure 93 show where the spikes take place in the pulses. Unfortunately, these spikes take place outside of the main envelope, where the pulse is highly attenuated. These are ultimately not useful for frequency detection.

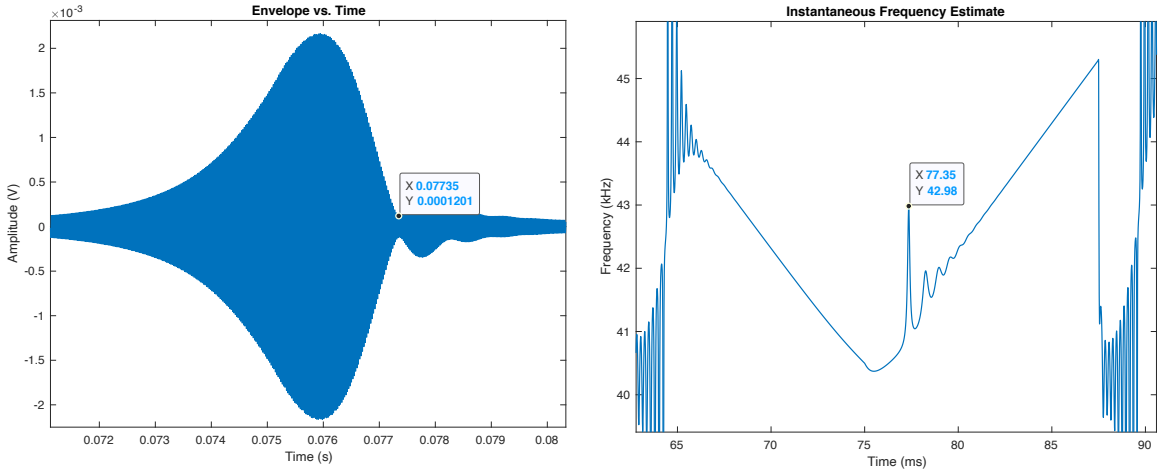


(a) (b)

Figure 92: The marked point in the pulse is where the spike takes place in the instantaneous frequency plot (Hilbert transform) for a 50ms halfway down and halfway up sweep signal

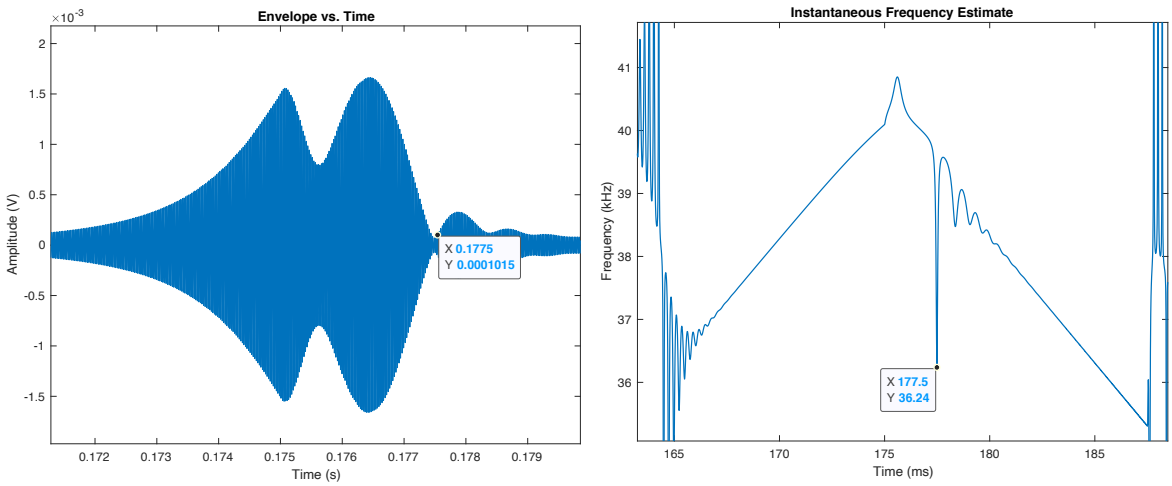


(a) (b)

Figure 93: The marked point in the pulse is where the spike takes place in the instantaneous frequency plot (Hilbert transform) for a 50ms halfway up and halfway down sweep signal

6.3. Explore Transmitting Signals that are Time Reversals of the Impulse Response

In order to have the best possible output signal from the transducer pair, the input signal should be designed to match the channel. According to Guimaraes [42], the output of the matched filter can be determined by:

$$y(t) = x(t) * h(t) \tag{6.1}$$

The convolution integral for $y(t)$ can be written as:

$$y(t) = \int_0^t x(\tau)h(t-\tau)d\tau \tag{6.2}$$

The impulse response $h(t)$ can be matched by $kg(t)$. Letting $k = 1$ for simplicity, $h(t) = g(t)$. Substituting $h(t)$ by $g(T-t) = g[-(t-T)]$ gives:

$$y(t) = \int_0^t x(\tau)\, g[-(t-T-\tau)]d\tau \tag{6.3}$$

At $T$, $y(t) = \int_0^T x(\tau)\, g(\tau)d\tau$ . Using a time reversal of the impulse response $h(t)$, we can see that it matches the filter. Figure 94 shows the time reversed impulse response.

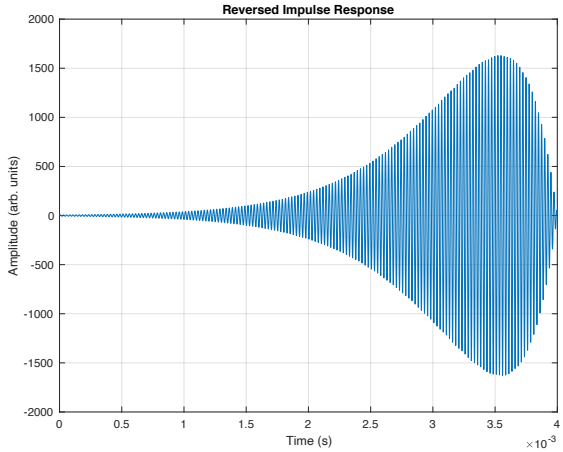


Figure 94: Time reversed impulse response of the fourth order filter representing the transducer pair

Using the $g(\tau)$ as the time reversed signal that is optimal for this filter, it is passed through the fourth order bandpass filter. The plot is shown in figure 95. This shows the optimal pulse formed from the time reversed signal.

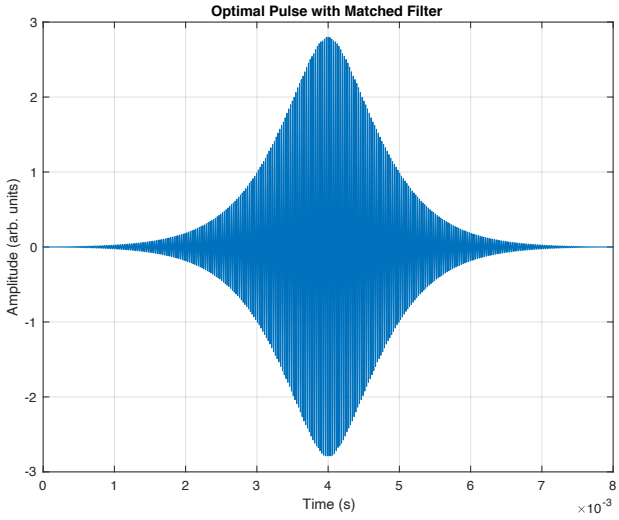


Figure 95: Optimal output pulse of time reversed channel g(t) filtered through fourth order bandpass filter

Although this was not largely considered in this work, it could be interesting to drive the ultrasonic transducer pair with an optimized signal designed for the channel.

## 6.4. New Method for Calculating Instantaneous Frequency

Throughout this work, two methods were used to measure instantaneous frequency – the Hilbert transform, and the zero-crossings method. Both of these methods had advantages and disadvantages. The Hilbert transform was highly accurate because it accounted for every sample in the entire signal. However, it did not perform well with noisy signals and therefore could not be used for measured data. Additionally, the Hilbert transform method does not work for clipped signals, as it only works on sinusoids. The zero-crossings method down sampled the signal heavily by only counting transitions and disregarding the rest of the samples. However, the zero-crossings method worked well for measured data and was a reliable and robust source of measurement.

Ideally in this work, a new method for measuring instantaneous frequency needs to be developed as neither of these two methods is perfect. The new method should be some combination of these two.

# Chapter 7

# CONCLUSION

This work explores the idea of using ultrasonic transducers in an indoor positioning system. There are four distinctive signal sweeping patterns that are designed to be uniquely identified by the receiver. Distance is meant to be calculated using ToF information, which is gathered by measuring the time for a frequency to leave the transmitter and be detected at the receiver. By measuring the instantaneous frequency at both the transmitter and receiver, a specific frequency can be identified in time. However, this method cannot be used since the instantaneous frequency gets distorted due to nonlinear phase characteristics of the transducers. This distortion results in a timing error, which would therefore impact the accuracy of ToF measurements. Two methods were used for measuring instantaneous frequency, the Hilbert transform and the zero-crossings method. The Hilbert transform was highly accurate but only worked for sinusoidal signals. The zero crossings method, developed in this work, was not as precise but was highly robust as it could work with any kind of signal. The hardware implementation included a PLL to receive and detect the signals from the transducer transmitter and receiver pair. The PLL was useful in detecting and "locking" on the signals within a specific range. The VCO of the PLL had a frequency that tracked the pulse's frequency when the PLL was locked. This allowed for accurate instantaneous frequency detection, only within a narrow bandwidth surrounding the center frequency of the transducers. Deviations or artefacts appeared in the instantaneous frequency plots. This was a result of nonlinear phase characteristics in the transducer transmitter and receiver pair. This was confirmed in both simulations as well as experimental results. Because of how highly localized some of these deviations were, they were considered for use in accurate pulse detection. However, most of the spikes observed in this work took place in attenuated portions of the pulses and were not considered to be useful. One simulation and measurement of a chirp signal with phase discontinuity at the center frequency indicated that the deviation could be detected and used for frequency detection. Further exploration of frequency sweeping patterns could illuminate how these spikes can be created within the pulse and be used for frequency detection. It is important for them to take place near the center frequency of 40kHz in order to have a large enough magnitude for significant signal processing.

WORKS CITED


[1] "Ultrasonic Transducers Technical Notes." Olympus NDT, 2006, [Online]. Available: https://mbi-ctac.sites.medinfo.ufl.edu/files/2017/02/ultrasound-basics.pdf.

[2] K. G. Panda, D. Agrawal, and A. Nshimiyimana, "Effects of environment on accuracy of ultrasonic sensor operates in millimetre range," *Perspect. Sci.*, vol. 8, 2016, [Online]. Available: https://reader.elsevier.com/reader/sd/pii/S221302091630163X?token=C282D3FAEB61BF69367CC0B03D84695A6F1106BB56E5BD0CC7C1B85D765F00E11687C1894AAB73E49EB71F3E8164359F.

[3] J. Zixi and B. Guan, "Received signal strength difference-based tracking estimation method for arbitrarily moving target in wireless sensor networks," *Int. J. Distrib. Sens. Netw.*, vol. 14, 2018, [Online]. Available: https://doi.org/10.1177/1550147718764875.

[4] G. V. Zàruba, M. Huber, F. A. Kamangar, and I. Chlamtac, "Indoor Location Tracking Using RSSI Readings from a Single Wi-Fi Access Point," *Springer-Verl.*, vol. 13, no. 2, pp. 221–235, 2007, doi: 10.1007/s11276-006-5064-1.

[5] W. van Schaik, M. Grooten, T. Wernaart, and C. van der Geld, "High Accuracy Acoustic Relative Humidity Measurement in Duct Flow with Air," *Sensors*, vol. 10, no. 8, pp. 7421–7433.

[6] G. Jones and M. W. Holderied, "Bat echolocation calls: adaptation and convergent evolution," *R. Soc.*, Jan. 2007, [Online]. Available: https://royalsocietypublishing.org/doi/full/10.1098/rspb.2006.0200.

[7] D. S. Edwards, R. Allen, T. Papadopoulos, D. Rowan, K. S.Y., and L. Wilmot-Brown, "Investigations of mammalian echolocation," *IEEE*, Sep. 2009, [Online]. Available: https://ieeexplore-ieee-org.ezproxy.lib.calpoly.edu/stamp/stamp.jsp?tp=&arnumber=5335313.

[8] J. F. Havlice and J. C. Taenzer, "Medical Ultrasonic Imaging: An Overview of Principles and Instrumentation," *IEEE*, vol. 67, no. 4, pp. 620–641, 1979.

[9] R. W. Cootney, "Ultrasound Imaging: Principles and Applications in Rodent Research," *ILAR J.*, vol. 42, no. 3, pp. 233–247, 2001.

[10] P. Sprawls, "Ultrasound Production and Interactions," *The Physical Principles of Medical Imaging*. http://www.sprawls.org/ppmi2/USPRO/#Transducer.

[11] J. Forlizzi and C. DiSalvo, "Service Robots in the Domestic Environment: A Study of the Roomba Vacuum in the Home," *Proc. 1st ACM SIGCHISIGART Conf. Hum.-Robot Interact.*, 2006.

[12] M. Montemerlo, J. Pineau, N. Roy, S. Thrun, and V. Verma, "Experiences with a mobile robotic guide for the elderly," *AAAI/IAAI*, 2002.

[13] "Ultrasonic Distance Sensor - 3V or 5V - HC-SR04 compatible - RCWL-1601," *adafruit*. .

[14] "Ultrasonic Flowmeter Technology," *Universal Flow Monitors, Inc.* https://www.flowmeters.com/product-list.php?page=ultrasonic-technology/pg1-cid100.html=/asc_action=SetCurrCat/category_id=100.

[15] "How Does Ultrasonic Clamp-on Technology Work?," *Badger Meter*. https://www.badgermeter.com/how-does-ultrasonic-clamp-on-technology-work/.

[16] “Ultrasonic Transit-Time Measurement,” *Lauris Technologies*. http://www.lauristech.com/technologies_type/ultrasonic-transit-time-measurement/.

[17] L. Segers, D. Van Bavegem, S. De Winne, A. Braeken, A. Touhafi, and K. Steenhaut, “An ultrasonic multiple-access ranging core based on frequency shift keying towards indoor localization,” *Sensors*, vol. 15, no. 8, 2015.

[18] H. Yucel, T. Ozkir, R. Edizkan, and A. Yazici, “Development of indoor positioning system with ultrasonic and infrared signals,” *Int. Symp. Innov. Intell. Syst. Appl.*, pp. 1–4, 2012.

[19] T. A. Bigelow, “Experimental Evaluation of Nonlinear Indices for Ultrasound Transducer Characterizations,” Colorado State University.

[20] V. A. Marathe, “Analog Single Sideband-Pulse Width Modulation Processor for Parametric Acoustic Arrays,” California Polytechnic State University, San Luis Obispo.

[21] “Ultrasonic Sensor Set 40Khz Transmitter and Receiver.” Jameco, [Online]. Available: https://www.jameco.com/Jameco/Products/ProdDS/139492.pdf.

[22] “The Unit Impulse Response,” *LPSA (Linear Physical Systems Analysis)*. .

[23] M. Stéphane, “CHAPTER 4 Time Meets Frequency,” in *A Wavelet Tour of Signal Processing*, Elsevier.

[24] A. E. Hassanien, K. Shaalan, T. Gaber, and M. F. Tolba, *Proceedings of the International Conference on Advanced Intelligent Systems and Informatics 2017*, vol. 533. Springer, 2016.

[25] J. Mier, A. Jaramillo-Alcázar, and J. J. Freire, “t a Glance: Indoor Positioning Systems Technologies and Their Applications Areas,” in *Information Technology and Systems*, vol. 918, Springer, 2019.

[26] B. Huang and Y. Gao, “Integrated Indoor Positioning with Mobile Devices for Location-Based Service Applications,” presented at the Database Systems for Advanced Applications. DASFAA 2014, Bali, Indonesia, 2014, vol. 8505, pp. 329–341.

[27] H. Liu, H. Darabi, J. Liu, and Banerjee, “Survey of Wireless Indoor Positioning Techniques and Systems,” *IEEE*, vol. 37, no. 6, pp. 1067–1080, Nov. 2007.

[28] V. Kindratenko, “A Comparison of the accuracy of an Electromagnetic and a Hybrid Ultrasound-Inertia Position Tracking System,” *Presence*, vol. 10, no. 6, pp. 657–663.

[29] C. Y. Chan and R. J. Knight, “Laboratory measurementsof electromagneticwave velocity in layered sands,” *Water Resour. Res.*, vol. 37, no. 4, pp. 1099–1105, Apr. 2001.

[30] J. Schaefer, “Trilateration Versus Triangulation for Indoor Positioning,” *New Technologies*, Nov. 28, 2018. .

[31] K. Yu, I. Sharp, and Y. J. Guo, “Position Calculation,” in *Ground-Based Wireless Positioning*, Wiley, 2009, p. 150.

[32] M. Schwartz, “Multiple access techniques: FDMA, TDMA, CDMA; system capacity comparisons,” in *Mobile Wireless Communications*, Cambridge: Cambridge University Press, 2004, pp. 137–160.

[33] F. R. Chung, J. A. Salehi, and V. K. Wei, “Optical orthogonal codes: design, analysis and applications,” *IEEE Trans. Inf. Theory*, vol. 35, no. 3, 1989.

[34] D. Nelson, “Special purpose correlation functions for improved signal detection and parameter estimation,” *IEEE Int. Conf. Acoust. Speech Signal Process.*, vol. 4, no. IEEE.

[35] “An introduction to Spread-Spectrum Communications.” Maxim Integrated Products, Inc., 2003, [Online]. Available: https://www.maximintegrated.com/en/design/technical-documents/tutorials/1/1890.html.

[36] “Understanding Spread Spectrum for Communications,” *National Instruments*, Mar. 2019. .

[37] K. Rouabah, S. Attia, R. Harba, P. Ravier, and S. Boukerma, “Optimized Method for Generating and Acquiring GPS Gold Codes,” *Hindawi*, vol. 2015, pp. 1–9, 2015.

[38] B. Tian and H.-U. Schnitzler, “Echolocation signals of the Greater Horseshoe bat (Rhinolophus ferrumequinum) in transfer flight and during landing,” *J. Acoust. Soc. Am.*, vol. 101, no. 4, pp. 2347–2364.

[39] M. Pollakowski, H. Ermert, L. Von Bernus, and T. Schmeidl, “The optimum bandwidth of chirp signals in ultrasonic applications,” *Ultrasonics*, vol. 31, no. 6, pp. 417–420, 1993.

[40] B. Boashash, “Estimating and interpreting the instantaneous frequency of a signal. I. Fundamentals,” *IEEE*, vol. 80, no. 4, pp. 520–538, Apr. 1992, doi: 10.1109/5.135376.

[41] C. Mendina, J. C. Segura, and Á. De la Torre, “Ultrasound Indoor Positioning System Based on a Low-Power Wireless Sensor Network Providing Sub-Centimeter Accuracy,” *Sensors*, vol. 13, no. 3, pp. 3501–3526, 2013.

[42] D. A. Guimaraes, *Digital transmission: a simulation-aided introduction with VisSim/Comm*. Springer Science & Business Media.

[43] P. Lazik and A. Rowe, “Indoor Pseudo-ranging of Mobile Devices using Ultrasonic Chirps,” *Assoc. Comput. Mach.*, pp. 99–112, 2012, doi: 10.1145/2426656.2426667.

[44] M. Roche, “Time Synchronization in Wireless Networks.” https://www.cse.wustl.edu/~jain/cse574-06/ftp/time_sync/index.html.

[45] K. Huang, California Polytechnic State University, San Luis Obispo, 2020.

[46] “Oscilloscope Preamplifier LNA10,” *AlphaLab Inc.* https://www.alphalabinc.com/product/lna10/.

[47] “LMC567 Low-Power Tone Decoder.” Dec. 2015, [Online]. Available: http://www.ti.com/lit/ds/symlink/lmc567.pdf?&ts=1589060523390.

[48] R. Klukas and M. Fattouche, “Line-of-sight angle of arrival estimation in the outdoor multipath environment,” *IEEE Trans. Veh. Technol.*, vol. 47, no. 1, pp. 342–351.

[49] P. J. Allisy-Roberts and J. Williams, “Chapter 9 - Imaging with ultrasound,” in *Farr’s physics for medical imaging*, 2007.

[50] “Antenna Theory- Near and Far Fields,” *Tutorials point*. https://www.tutorialspoint.com/antenna_theory/antenna_theory_near_and_far_fields.htm.

[51] R. Paschotta, “Dispersion,” *Encyclopedia of Laser Physics and Technology*. RP Photonics.

[52] U. Keller and L. Gallmann, “Ultrafast Laser Physics,” 1999, p. 1507.

APPENDIX

A. Code to generate 200ms signal with 100ms linear up chirp

```
%sweep up 35k-45k
%200msupinterpolation
t = 0:1e-6:0.1;
y=chirp(t, 35000, t(end), 45000);
y=round(y, 6);
csy = csapi(t,y);
csycoefs = csy.coefs(:,4);

samples= 0:1e-6:0.05;
a=cos(2*pi*35000.*samples-(pi));
b=cos(2*pi*45000.*samples);

csa= csapi(samples, a);
csacoefs = csa.coefs(:,4);
csb = csapi(samples, b);
csbcoefs = csb.coefs(:,4);

sweep= [csa csy csb];
sweepdouble = sweep.coefs

outsweep = vertcat(sweep.coefs)
outsweep = outsweep(:,4);
```

B. Code to generate instantaneous frequency plot by measuring zero crossings

```
%vco data imported from oscilloscope
comparator = [];
time = [];
freq = [];


for i=2:length(vco(1:100000))
    if(vco(i)>0)
        comparator(end+1)=1;
    else
        comparator(end+1)=-1;
    end
end


for m=2:length(comparator(1:99999))
    if (comparator(m)-comparator(m-1)) < -1
            time(end+1)= t(m);
    end
end

for s=2:length(time)
        freq(end+1) = 1/(time(s)-time(s-1));
end
```

C. Code to generate discrete time transfer function for fourth order bandpass filter

```
w1= 2*pi*40294.8;
q1= 55.94;
w2= 2*pi*40289.2;
q2=57.95;
k = (w1/q1)*(w2/q2);
z = [0 0];
p1= roots([1 w1/q1 w1^2]);
p2= roots([1 w2/q2 w2^2]);
p= reshape([p1 p2], [1, 4]);

[b, a] = zp2tf(z', p', k);
H = tf(b,a); %continuous time transfer function
fs = 1e6;
Hd = c2d(H, 1/fs) %convert to discrete time transfer function

poled = pole(Hd);
zerod = zero(Hd);
Kd = 2.4709e-8;
[bd, ad] = zp2tf(zerod, poled, Kd); %convert zeros and poles to tf form

y = filter(bd,ad,signal); %pass signal through filter
```

D. Nonlinear phase components and Dispersion

In figure 96a, the signal spectrum is shown in red, while the spectral phase is shown in black. The non-linear phase component skews the output pulse as a result of dispersion. Dispersion is the dependence of the phase velocity in a medium on frequency or propagation mode [51]. This phenomenon is true in both optics and acoustics. In addition to having a frequency dependent phase characteristic, dispersion also separates a wave into its component frequencies. In figure 96b the wave's higher frequency components are spread out to the right. This feature was similarly observed in simulation results and explains why there are smaller pulses on the higher frequency end of the chirp signals in an envelope.

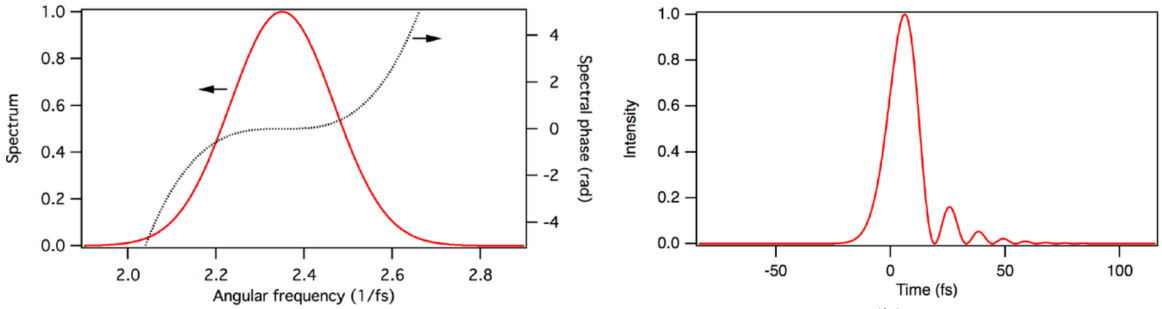


(a) (b)

Figure 96: Spectrum and phase (a) and magnitude of spectrum with non-linear phase (b) [52]

E. Sweeping patterns with abrupt changes at 40kHz

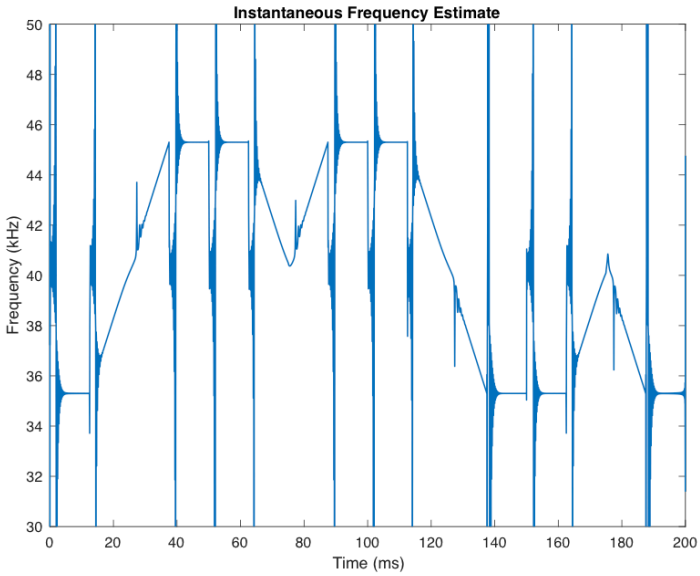


Figure 97: These four sweeping rates were initially tested to be used in this work. These sweeps were up, halfway down and halfway up, down, and halfway up and halfway down. At this rate, the artefacts in each of the sweeping patterns can be observed.

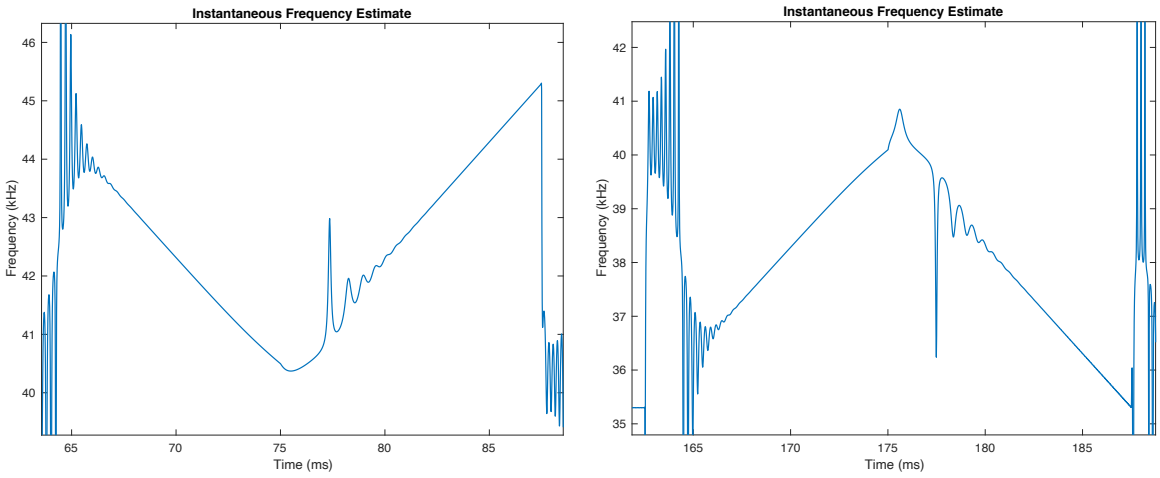


(a) (b)

Figure 98: The instantaneous frequency measurements of halfway down and halfway up (a) and halfway up and halfway down (b) are shown. These plots show artefacts similar to what was seen for the up and down sweep signals.